Journal of Human Evolution 172 (2022) 103252

Contents lists available at ScienceDirect

Journal of Human Evolution

journal homepage: www.elsevier.com/locate/jhevol

Two Late Pleistocene human femora from Trinil, Indonesia: Implications for body size and behavior in Southeast Asia

Christopher B. Ruff [a, *], Adam D. Sylvester [a], Neni T. Rahmawati [b], Rusyad A. Suriyanto [b], Paul Storm [c], Maxime Aubert [d], Renaud Joannes-Boyau [e, f], Harold Berghuis [g], Eduard Pop [h], K. Joost Batenburg [h], Sophia B. Coban [i, 1], Alex Kostenko [i], Sofwan Noerwidi [j], Willem Renema [g, k], Shinatria Adhityatama [d], Josephine C. Joordens [g, l]

[a] Center for Functional Anatomy and Evolution, Johns Hopkins University, USA
[b] Laboratory of Bioanthropology and Paleoanthropology, Universitas Gadjah Mada, Indonesia
[c] Groningen Institute of Archaeology, University of Groningen, the Netherlands
[d] Griffith Centre for Social and Cultural Research, Griffith University, Australia
[e] Geoarchaeology and Archaeometry Research Group (GARG), Southern Cross University, Lismore, New South Wales, Australia
[f] Centre for Anthropological Research, University of Johannesburg, Johannesburg, Gauteng Province, South Africa
[g] Naturalis Biodiversity Center, Leiden, the Netherlands
[h] Leiden Institute of Advanced Computer Science, Leiden University, the Netherlands
[i] Centrum Wiskunde & Informatica, Science Park 123, 1098 XG Amsterdam, the Netherlands
[j] Research Center for Archaeometry, National Research and Innovation Agency, Indonesia
[k] Institute for Biodiversity and Ecosystems Dynamics, University of Amsterdam, the Netherlands
[l] Faculty of Science and Engineering, Maastricht University, the Netherlands

ARTICLE INFO

Article history:
Received 31 May 2022
Accepted 15 August 2022
Available online xxx

Keywords:
Femur
Postcrania
Homo
Cross-sectional geometry
Body mass

ABSTRACT

Late Pleistocene hominin postcranial specimens from Southeast Asia are relatively rare. Here we describe and place into temporal and geographic context two partial femora from the site of Trinil, Indonesia, which are dated stratigraphically and via Uranium-series direct dating to ca. 37–32 ka. The specimens, designated Trinil 9 and 10, include most of the diaphysis, with Trinil 9 being much better preserved. Microcomputed tomography is used to determine cross-sectional diaphyseal properties, with an emphasis on midshaft anteroposterior to mediolateral bending rigidity (I_x/I_y), which has been shown to relate to both body shape and activity level in modern humans. The body mass of Trinil 9 is estimated from cortical area and reconstructed length using new equations based on a Pleistocene reference sample. Comparisons are carried out with a large sample of Pleistocene and Holocene East Asian, African, and European/West Asian femora. Our results show that Trinil 9 has a high I_x/I_y ratio, most consistent with a relatively narrow-bodied male from a mobile hunting-gathering population. It has an estimated body mass of 55.4 kg and a stature of 156 cm, which are small relative to Late Pleistocene males worldwide, but larger than the penecontemporaneous Deep Skull femur from Niah Cave, Malaysia, which is very likely female. This suggests the presence of small-bodied active hunter-gatherers in Southeast Asia during the later Late Pleistocene. Trinil 9 also contrasts strongly in morphology with earlier partial femora from Trinil dating to the late Early-early Middle Pleistocene (Femora II–V), and to a lesser extent with the well-known complete Femur I, most likely dating to the terminal Middle-early Late Pleistocene. Temporal changes in morphology among femoral specimens from Trinil parallel those observed in *Homo* throughout the Old World during the Pleistocene and document these differences within a single site.

1. Introduction

Hominin postcranial remains from the Late Pleistocene are relatively rare in Southeast Asia (Santa Luca, 1980; Baba et al., 1990;

* Corresponding author.
E-mail address: cbruff@jhmi.edu (C.B. Ruff).
[1] Present address: Department of Mathematics, The University of Manchester, UK.

https://doi.org/10.1016/j.jhevol.2022.103252
0047-2484/

Brown et al., 2004; Détroit et al., 2004, 2019; Shackelford and Demeter, 2012; Curnoe et al., 2019). Recent discoveries have increased the range of variation in both body size (Brown et al., 2004; Détroit et al., 2013) and potentially locomotor behavior (Jungers et al., 2009a; Détroit et al., 2019) among Late Pleistocene populations from this region. The significance of archaic vs. modern postcranial morphology, in terms of both behavior and ancestry, has also been a topic of ongoing discussion for Late Pleistocene Southeast Asia and East Asia as a whole (Tocheri et al., 2007; Jungers et al., 2009a,b; Shang and Trinkaus, 2010; Curnoe et al., 2015, 2019; Xing et al., 2018; Wei et al., 2020, 2021).

Here we describe and place into temporal and regional context two Late Pleistocene partial femora, designated Trinil 9 and 10, from the site of Trinil on Java, Indonesia. The specimens were discovered by T. Jacob in 1978 and were included in some later compendia of Indonesian fossil hominin specimens (de Lumley, 1993; Indriati, 2004). However, aside from a few metrics included in a brief comparative analysis (Grimaud-Hervé et al., 1994), they have remained undescribed and largely unknown. The indicated discovery location (Widiasmoro, 1991) was recently identified as a Late Pleistocene fluvial terrace, provisionally—through stratigraphic correlation—assigned an age of 31 ± 6 ka (Berghuis et al., 2021). This would make them part of only a very small number of adult femora known from Late Pleistocene Southeast Asia, the others being the Deep Skull femur from Niah Cave, Malaysia (Curnoe et al., 2019, 2021), fragmentary remains from Wajak, Indonesia (Storm, 1995), and the Terminal Pleistocene sample from Tam Hang, Laos (Shackelford and Demeter, 2012).

Dubois' early discoveries at Trinil played a pivotal role in the development of hominin paleontology (Theunissen, 1989). In addition to the famous calotte and Femur I, which formed the basis for defining the taxon *Pithecanthropus erectus* (Dubois, 1894), four other femora (II–V) from Trinil were later identified by him among museum collections (Dubois, 1932, 1934; see Table 1). Based on both morphological comparisons (Ruff et al., 2015b) and new stratigraphic and dating analyses (Hilgen et al., in prep.; Pop et al., in prep.), it now appears that Femur I is significantly younger than the calotte and Femora II–V. Femora II–V and the calotte derive from Early or Middle Pleistocene fossiliferous beds, whereas Femur I derives from younger terrace deposits, probably dating to around the Middle to Late Pleistocene boundary (Hilgen et al., in prep.; Pop et al., in prep.).

The inclusion of the two new femora described herein, Trinil 9 and 10, expands the temporal range of specimens recovered from the Trinil site and allows further investigation of temporal trends in morphology in this region. We also include broader comparisons of femoral structural properties and reconstructed body size with a large sample of other Pleistocene and more recent *Homo* from East Asia, Africa, and Europe/West Asia. We aim to assess long-term temporal trends as well as regional differences in these characteristics, and address their implications for the evolution of postcranial morphological variation within *Homo*.

Table 1
Femora discovered at Trinil.

Trinil #	Femur #	Discovery	First description
3	I	Dubois, 1892	Dubois, 1893
6	II	Dubois, 1900	Dubois, 1932
7a	III	Dubois, 1900	Dubois, 1932
8	IV	Dubois, 1900	Dubois, 1932
7b	V	Dubois, 1900	Dubois, 1934
9		Jacob, 1978	Grimaud-Hervé et al., 1994
10		Jacob, 1978	Grimaud-Hervé et al., 1994

2. Materials and methods

2.1. Trinil 9 and 10 femora

Photographs of the Trinil 9 and 10 specimens are shown in Figure 1. Both are from the right side and are missing proximal and distal ends. Trinil 9 is more complete, extending from the intertrochanteric region to near the distal end of the diaphysis (more details are given in sections 2.5 and 3.1). Trinil 10 is broken somewhat distal to the lesser trochanter, with a small proximally projecting spike, and does not extend as far distally. Total preserved lengths, as measured here, are 307 mm (Trinil 9) and 283 mm (Trinil 10). Both specimens are currently housed in the Laboratory of Bioanthropology and Paleoanthropology at the Gadjah Mada University in Yogyakarta (Indonesia).

It should be noted that a dual numbering system has been used for the Trinil femora, as indicated in Table 1, with both Trinil numbers and 'Femur' numbers (designated with Roman numerals) used for the first five femora discovered from the site. There has been some variation over the years in the correspondence between the two systems (Jacob, 1973, 1975, 1978; de Lumley, 1993). Here we follow the numbering scheme of Grimaud-Hervé et al. (1994) and Indriati (2004), and do not assign a 'Femur' number to Trinil 9 and 10. We do use the 'Femur' numbers for the previously discovered femora, as these have been most commonly used in past considerations of these specimens (e.g., Dubois, 1932, 1934; Day and Molleson, 1973; Kennedy, 1983; Ruff et al., 2015b).

2.2. Provenience

The Trinil 9 and 10 femora were discovered by Teuku Jacob in 1978 along the right bank of the Solo River close to Trinil, just south of the Trinil Museum and opposite to the left bank site where Dubois excavated the other hominin femora, skullcap, and teeth (Fig. 2). Recent studies have shown that the Trinil area has a complex geological build-up, consisting of Early to Middle Pleistocene volcaniclastic deposits overlain and incised by younger terrace-related deposits, forming a landscape of seven fluvial terraces (T7 to T1) dating back to ~300 ka (Berghuis et al., 2021).

Trinil 9 and 10 were found in isolated remnants of a lower fluvial terrace on the opposite side of the river, which is the youngest terrace of the Trinil area (terrace T1; Fig. 2). The terrace surface has a height of ~50 m above mean sea level, which is ca. 8 m above low water level of the river. Terrace T1 is a fill terrace made up of loosely consolidated ash, dominated by vitric grains and monocrystalline feldspars, showing fine cross-bedding and stacked shallow channel structures. For this terrace, no direct dating results are available. However, Berghuis et al. (2021) correlated the terrace sequence of Trinil with the well-dated fluvial terraces in the Kendeng area (Rizal et al., 2020), ca. 18 km downstream, referring to position within the terrace sequence, composition of terrace sediments and available luminescence-age of the T2 terrace in nearby Ginseng. It was found that Trinil terrace T1 correlates with the youngest terrace (Nglebak terrace) of the Kendeng area, which has been luminescence-dated to 31 ± 6 ka.

2.3. Uranium-series dating

Uranium-series dating on the Trinil bone fragments was carried out by measuring several isotopes of the ^{238}U decay chain, including ^{238}U, ^{234}U, and ^{230}Th. In addition, other isotopes not part of the ^{238}U decay sequence such as ^{232}Th and ^{235}U were measured to account for detrital thorium contamination or to confirm natural abundance ratios, respectively. Trinil 9 and Trinil 10 were sampled by M. Aubert in the Laboratory of Bioanthropology and

Figure 1. Photographs of Trinil 9 and 10 femora. Proximal is to the right. Scale bar is 5 cm. Arrows indicate longitudinal positions of proximal and distal landmarks for Segment 2 distance used in length reconstruction.

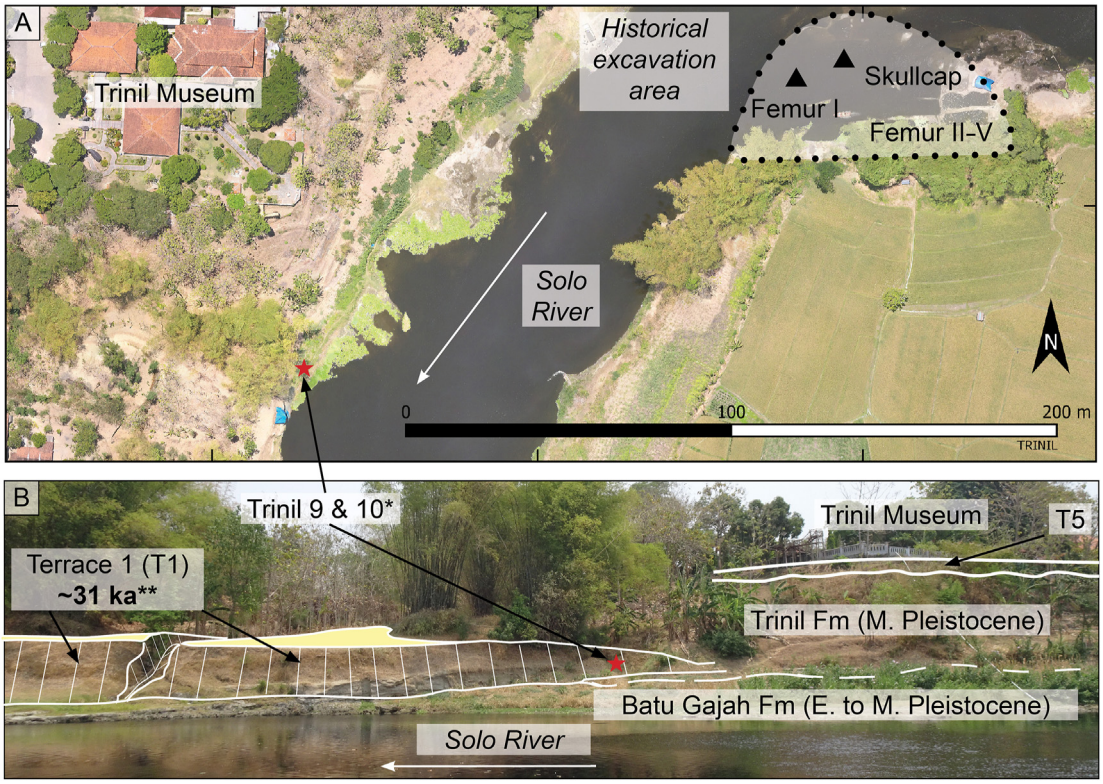

Figure 2. Provenience of Trinil 9 and Trinil 10. A: The Solo River around Trinil, with the Dubois excavation site on the left bank and the discovery site of Trinil 9 and 10 on the right bank. B: View of the river bank and discovery site of Trinil 9 and 10 with annotated stratigraphy. See Berghuis et al. (2021) for stratigraphic details. **The ~31 ka age of terrace T1 is based on a correlation with dated terraces 18 km downstream (Rizal et al., 2020). *Uranium-series age of Trinil 10 (this study) yielded a minimum age of 32 ka. Fm = formation; M. = Middle; E. = Early.

Paleoanthropology, Universitas Gadjah Mada, Indonesia (where T9 and T10 are curated), using an electric cutting device to obtain a small fragment from both femora. Uranium-series measurements on Trinil 9 and 10 bone fragments were obtained using an ESI NW213 laser ablation instrument coupled to an MC-ICPMS Neptune XT and an Agilent 7700 ICPMS at the BIOMICS laboratory, Geoarchaeology and Archaeometry Research Group (GARG) of Southern Cross University. Bones were first sectioned and polished to a 5 μm smoothness before being placed in the ablation chamber for analyses. Each fragment was measured by a succession of rasters beginning at the outer edge of the bones and moving toward the center. Each raster was measured with the following parameters: 1200 μm in length, a spot size of 110 μm, a translation speed of 5 μm per second, and an average energy of 5.15 J/cm^2. ^{234}U and ^{230}Th were measured simultaneously, with uranium in the center faraday cup coupled with a secondary electron multiplier and thorium in the L3 faraday cup coupled to an ion counter. All other faraday cups were set to use high-gain 10^{11} Ω amplifiers. Baseline and drifts were corrected using NIST 610 and NIST 612 glass standards, whereas two corals (the MIS7

Faviid and MIS5 Porites corals from the Southern Cook Islands; Woodroffe et al., 1991) were used to correct $^{234}U/^{238}U$ and $^{230}Th/^{238}U$ ratios and assess the accuracy of measurements. To account for potential matrix effects, a fossil rhinoceros tooth fragment from Africa with known and homogenous isotope concentrations was used as a matrix match standard. (For more information about the analytical protocol, see Grün et al., 2008; Herries et al., 2018.)

2.4. Cross-sectional analyses

Trinil 9 and 10 were μCT scanned using the custom-built and highly flexible CT scanner, FleX-ray scanner, developed by TESCAN-XRE NV located at Centrum Wiskunde & Informatica, Amsterdam, The Netherlands. The apparatus consists of a cone beam microfocus X-ray point source that projects polychromatic X-rays onto a 1944 × 1536 pixels, 14-bit, flat detector panel. The detector was vertically tiled to increase the pixel resolution. This process and more details of the apparatus are given in Coban et al. (2020). The spatial tiling returned a reconstruction volume with a voxel size of 35 μm^3. The data were collected over 360° in circular and continuous motion with projections distributed evenly over the full circle (2000 projections per detector tile). The scans were performed with a tube voltage of 70 kV and tube power of 50 W. The exposure time was 1050 ms per projection image.

For each femur, the associated μCT image stack was imported into Avizo Lite v. 9.0.1 (FEI Visualization Sciences Group, 2015) and a combination of thresholding and manual selection segmentation was used to generate a surface model. Standard anatomical axes were identified from the surface model following Ruff (2002), and these axes then were rotated to align with the virtual coordinate axes. This rotation transformation was applied to the image stack, which then was resampled at the original voxel dimensions. This transformation ensured that CT images were oriented perpendicular to the shaft axis. Transverse cross-sectional images were extracted at 20%, 35%, 50%, 65%, and 80% of a bone length dimension (length'—see below for derivation), measured from the reconstructed position of the distal end, following previous studies (Ruff and Hayes, 1983; Puymerail et al., 2012; Trinkaus and Ruff, 2012; Ruff et al., 2015b). As in an earlier study of Trinil partial femora (Ruff et al., 2015b), the 80% section was considered to lie 1.5 cm from the distal edge of the lesser trochanter. Together with the bone length estimate, this allowed placement of the other four cross sections. Any trabecular bone or matrix infill in the medullary cavity was manually removed from section images, and small cracks were filled in. External and internal cortical contours were well defined in all sections (see Fig. 3 below).

Cross-sectional diaphyseal structural properties were derived from CT images using the MomentMacro routine (Ruff, n.d.). Properties include bone areas, second moments of area, and section moduli, which can be used to assess axial, bending, and torsional rigidity and strength. Comparative analyses focus in particular on anteroposterior/mediolateral (A-P/M-L) bending rigidity of the 50% (midshaft) section, referred to as I_x/I_y (Ruff, 2019). This is in part because the 50% section is best represented among other available specimens and samples, and because this cross-sectional 'shape' property has been shown to reflect activity as well as body shape effects in past studies (Ruff, 1995; Weaver, 2003; Stock, 2006; Shaw and Stock, 2011; Wescott, 2014; Davies and Stock, 2014b; Ruff et al., 2015a). It should be noted that section moduli here are 'true' section moduli, calculated using the maximum distance from the neutral axis or centroid rather than half external diameters, which have been used in some previous studies (see Ruff, 2019 for a discussion of these differences).

2.5. Bone length and body size reconstruction

As in a previous study of Trinil femora I–V (Ruff et al., 2015b), maximum bone length in Trinil 9 was estimated using the general approach of Steele and McKern (1969), based on the distance between preserved landmarks on the diaphysis. Steele and McKern's Segment 2 measures the distance parallel to the long axis of the diaphysis from the center of the lesser trochanter to the point where the linea aspera begins to separate into medial and lateral supracondylar lines, both of which landmarks are clearly visible in the specimen (Fig. 1; the lesser trochanter position is based on the outline of its broken base). The maximum length was estimated from this distance using 10 available regression equations based on five different modern human populations—Mississippian Native Americans (Steele and McKern, 1969), Alaskan Inuits (Fellmann, 2004), European-Americans and African-Americans (Steele, 1970), and Neolithic and Mesolithic Europeans (Jacobs, 1992). The mean of the five estimates was used for Trinil 9. The same landmarks cannot be determined with any precision for Trinil 10, because of its proximal break distal to the lesser trochanter and extensive surface wear (Fig. 1; also see below), so no length reconstruction was attempted for this specimen. For locating cross sections, a dimension referred to as 'biomechanical length,' or length', taken as the distance along the long axis of the shaft from the proximal surface of the femoral neck to the average distal projection of the condyles (Ruff, 2002), was calculated from maximum femoral length using the formula: Length' = 0.9354 × Maximum length + 0.9 (Ruff et al., 2015b; lengths in mm).

Stature was reconstructed from femoral maximum length in Trinil 9 using five sets of equations based on a variety of modern reference samples: two Thai samples (Mahakkanukrauh et al., 2011; Gocha et al., 2013), South African Blacks (Feldesman and Lundy, 1988), Holocene Europeans (Ruff et al., 2012), and African 'Pygmies' (Hens et al., 2000). Four of the samples are from lower latitude populations whose limb length to stature proportions might be expected to better match those of Trinil 9 (Holliday and Ruff, 1997). All include small-bodied individuals whose femoral lengths overlap with that estimated for Trinil 9, except for African 'Pygmies,' who are shorter. Because, as shown later, Trinil 9 is likely to have been a male, male formulae were used, again except for African 'Pygmies' where only a mixed-sex sample equation was available. As in four cases Trinil 9 fell well within the size (length) range of the reference sample, ordinary least squares equations were used. Where this was not the case, in African 'Pygmies', a mean of four stature estimates generated from 'inverse' (ordinary least squares), 'classical,' reduced major axis, and major axis equations was calculated (Hens et al., 2000). Because one of the equations for the Thai samples was based on cadaveric statures (Mahakkanukrauh et al., 2011), 2.5 cm was subtracted to convert the estimate to living stature (Trotter and Gleser, 1952). Formula (1) from Raxter et al. (2006), with an age of 30 years (Ruff et al., 2019), was used to convert skeletal height to living height when using the other Thai sample equation (Gocha et al., 2013). All equations used to estimate maximum femoral length from Segment 2 length, and stature from maximum femoral length, are given in Supplementary Online Material (SOM) Table S1.

Lower limb articular breadths are the preferred dimensions for estimating body mass from hominin skeletal remains, for several reasons (Ruff et al., 2018), and are used here whenever possible in comparative samples (see below). However, because neither Trinil 9 nor 10 preserves an articulation, alternative methods were also explored for this study. We have previously argued that the use of diaphyseal breadth dimensions to estimate body mass can be problematic, because of known environmental effects (other than

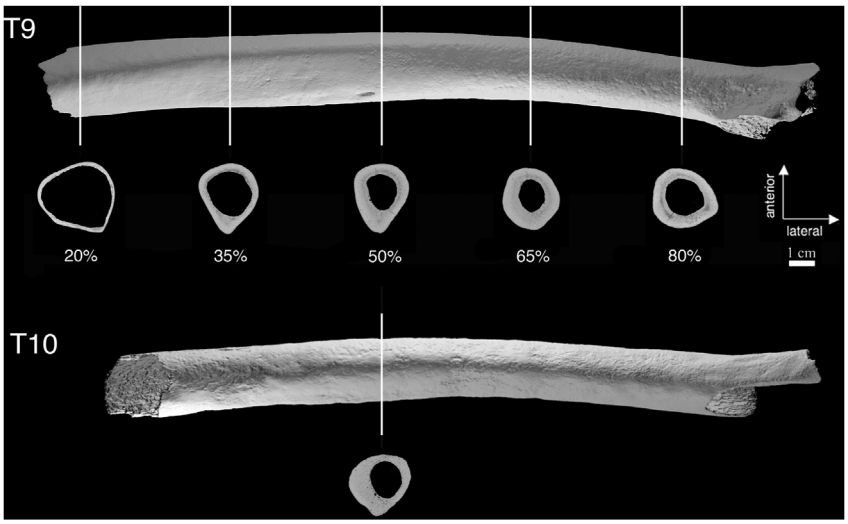

Figure 3. Three-dimensional rendering of Trinil 9 and 10 (medial views) from μCT scans, and extracted cross sections at percentages of reconstructed length' (see text). Proximal is to the right.

weight-bearing itself) on such dimensions, including activity level and relative muscularity (Ruff et al., 2018). These arguments apply in particular to non-*Homo* taxa, where large systematic differences in estimates are found when applying articular and diaphyseal-based equations (McHenry, 1992; Ruff et al., 2018). Within *Homo*, the largest systematic change in diaphyseal robusticity (strength relative to body size) occurs in the Holocene, as populations became more sedentary (e.g., Ruff et al., 2015a), with relatively little variation among Pleistocene samples (Trinkaus and Ruff, 2012; Friedl et al., 2016). Several previous studies have used primarily or exclusively Holocene samples to develop equations for estimating body mass from diaphyseal dimensions (Rightmire, 1986; Grabowski et al., 2015; Will and Stock, 2015). Here we avoid potential problems with such an approach by limiting our reference sample to Pleistocene *Homo* specimens with body mass estimates determined from lower limb articular breadths.

We also base our regression equations on cortical area (CA) rather than diaphyseal external dimensions. CA should reflect axial compressive loads, which in turn should be proportional to body mass (Ruff, 2019). Systematic variation in the relative thickness of long bone cortices within Pleistocene and Holocene *Homo* is well known (e.g., Ruff et al., 1993), and is not accounted for in external dimensions alone, but is reflected in CA. Second moments of area and section moduli are more heavily influenced by external dimensions and should be proportional to bending and torsional loads; thus, they would be expected to vary more with changes in activity level (Warden et al., 2014). The use of CA rather than these parameters as an estimator may therefore reduce such potentially confounding effects. In addition to CA, we also include bone length as another variable in multiple regression equations. Bone length alone is not advisable as a body mass predictor, because of marked differences in body proportions among Holocene and Pleistocene populations/taxa (Ruff, 1994; Davies and Stock, 2014a). But when combined with CA, it may provide additional information on body size that could be useful in body mass estimation (see Niskanen et al., 2018 for another example). We carry out least squares regressions of estimated body mass on midshaft femoral CA, and CA and maximum femoral length, in 69 Pleistocene *Homo* specimens, and compare their effectiveness using percent standard errors of estimate (%SEE) and average absolute percent prediction errors (%PE, calculated as $|(\text{observed} - \text{predicted})/\text{predicted}| \times 100$) as criteria.

Although, as noted earlier, stature estimates are derived for Trinil 9, the principal body size parameter evaluated here is body mass. This is in part because stature estimations are dependent on linear body proportions, which are impossible to evaluate directly in the new Trinil femora, but primarily because of the critical importance of body mass in many biological and ecological contexts (Calder, 1984; Schmidt-Nielson, 1984; Gardezi and da Silva, 1999; Brown and West, 2000). Several recent studies have evaluated body mass trends in *Homo* (Will and Stock, 2015; Jungers et al., 2016; Will et al., 2017, 2021; Ruff et al., 2018), and the present study allows further consideration of these trends, including in particular an assessment of variation within and between regions.

2.6. Comparative samples

Thirty-six Pleistocene femoral specimens from East Asia (defined as locations east of 90° E. latitude) used in comparative analyses are listed in Table 2. They range in age from ca. 900 to 14.5 ka, and geographically from northern China through Indonesia. In terms of both geographic location and period, the Deep Skull femur from Niah Cave, Malaysia (Borneo; 39–30 ka; Curnoe et al., 2019) and a partial femur from Wajak, Java, Indonesia (37.4–28.5 ka; Storm et al., 2013), are the closest to Trinil 9 and 10. In evaluating geographic proximity, it is important to realize that the present islands of Sumatra, Borneo, and Java were (intermittently) connected by land bridges ('Sundaland') to each other and to the Asian mainland during much of the Pleistocene, when the Sunda Shelf was not submerged (Voris, 2000; van den Bergh et al., 2016b; O'Connell et al., 2018). Thirty of the 36 femora have available cross-sectional diaphyseal properties for the femoral 50% section, whereas the other four have only body mass estimates, based on articular size (Table 2). Cross-sectional properties are also available for Tianyuan 1, but due to pathological distortion, they are not used in comparative analyses (see Supplementary Online Material [SOM] S1). However, the specimen is included as a data point in a plot of midshaft anteroposterior/mediolateral bending rigidity, for reference. Further details on all specimens, including references and properties used in analyses, are given in SOM Table S2 and SOM S1.

A total of 167 additional Pleistocene femora from sub-Saharan Africa and Europe/West Asia, listed in Table 3, were also included in broader comparative analyses. Eighty-six of these have cross-sectional dimensions, whereas the others were used only in body

Table 2
East Asian Pleistocene comparative specimens.

Specimen	Location	Date (ka)	BM/XS[a]
Kresna 11	Sangiran, Java, Indonesia	ca. 900	1/1
Trinil femora II, IV, V	Trinil, Java, Indonesia	830–773	3/3
Zhoukoudian femora I, II, IV, V, VI	Zhoukoudian, North China	770	5/5
Hualongdong 11	Central China	ca. 300	1/1
Jinnuishan 1	Northeast China	260	1/0
Trinil femur 1	Trinil, Java, Indonesia	140–90	1/1
Liujiang 1	Tongtianyan Cave, South China	139–67	1/1
Liang Bua 1	Flores, Indonesia	100–60	1/1
Tianyuan 1	Zhoukoudian, North China	40	1/(1)[b]
Zhoukoudian UC 67, 68, 105, 117	Zhoukoudian, North China	38.3–33.5	4/2
Wajak W-H-27	Java, Indonesia	37.4–28.5	1/0
Deep Skull femur	Niah Cave, Malaysia	39–30	1/1
Trinil 9, 10	Trinil, Java, Indonesia	37–32	1/1
Minatogawa 1, 2, 3, 4	Okinawa, South Japan	19.9	4/4
Tam Hang 2, 3, 7, 11, 13, 14, 22	Laos	15.7	7/6
Maomaodong GM7506, 7, 8	Southwestern China	14.5	3/3

[a] Number of individuals with body mass estimates/femoral cross-sectional dimensions. See SOM Table S2 for references and SOM S1 for additional information.
[b] Cross-sectional properties of Tianyuan 1 not included in analyses (see text, section 2.6, and SOM S1).

Table 3
African and European/West Asian Pleistocene comparative samples.

Region	Period	Date (ka)	Taxon/group	BM/XS[a]
Africa	Early Pleistocene	2035–1470	Early *Homo*	8/6
	Middle Pleistocene	700–160	*H. erectus*/MP archaic *Homo*	7/3
	Middle Pleistocene	385–236	*Homo naledi*	5/3
	Late Middle Pleistocene	195	Anatomically modern *H. sapiens*	1/0
	Late Late Pleistocene	25–20	Anatomically modern *H. sapiens*	4/0
Europe/W. Asia	Early Pleistocene	1770	Early *Homo*	1/0
	Middle Pleistocene	700–130	*H. erectus*/MP archaic *Homo*	25/11
	Late Pleistocene	110–36	LP archaic *Homo*	24/17
	Early Late Pleistocene	120–90	Anatomically modern *H. sapiens*	8/8
	Late Late Pleistocene	25–12	Anatomically modern *H. sapiens*	84/38

Abbreviations: MP = Middle Pleistocene; LP = Late Pleistocene.
[a] Number of individuals with body mass estimates/femoral cross-sectional dimensions. See SOM Table S3 for individual specimens and references and SOM S2 for additional information.

mass analyses. Ages range from 2.035 Ma to 12 ka. Further information on the samples and all individual properties are given in SOM Table S3 and SOM S2.

Finally, to provide a more recent comparative context, several Holocene samples, ranging from the Mesolithic through to living populations, were included from East Asia, sub-Saharan Africa, and Europe (Table 4). A total of 520 individuals and 104 sex/population means (for living samples) were included in body mass analyses, and 373 (skeletal) individuals in cross-sectional comparisons. For purposes of graphing, mean ages of 5000 years BP for the South African Late Stone Age sample and 3900 years BP for the Japanese Jomon sample were used in cross-sectional analyses. For body mass graphs, all early Holocene Africans (including the Gobero sample) were grouped together, with an average age of 6600 years BP. The living samples include a geographically wide range of populations from each region, derived mainly from Eveleth and Tanner (1976) and Ruff (1994). Most were measured in the mid-20th century, before the general worldwide increase in body mass characteristic of more recent populations (Katzmarzyk and Leonard, 1998). Further details are given in SOM Table S4 (skeletal samples), SOM Table S5 (living samples), and SOM S3.

Most comparisons are carried out as data plots of cross-sectional properties or body mass against time, with time represented on a logarithmic scale to better visualize more recent (Late Pleistocene–Holocene) trends. For regional comparisons, LOWESS nonparametric regression lines (Cleveland, 1979) are plotted through East Asian, African, and European/West Asian samples. For comparisons between the sexes, LOWESS regressions are plotted through males and females, for individuals with pelvic and/or cranially based sex assignments (or of known sex for very recent skeletal and living samples).[2] Sex differences within samples are

Table 4
Holocene comparative samples.

Region	Sample	Location	Date (yrs BP)[a]	BM/XS[b]
East Asia	Cau Giat	Vietnam	7500	5/0
	Jomon	Japan	5400–2400	156/33
	Recent skeletal	Japan	110	20/20
	Living	East Asia[c]	50	24/0
Africa	Gobero	Niger	9600–4400	16/0
	Late Stone Age	South Africa	10,000–2000	53/53
	Recent skeletal	Kenya, Uganda	80	40/40
	Living	Sub-Saharan Africa	50	43/0
Europe	Mesolithic	Europe	10,500–5900	74/74
	Recent skeletal	Europe	60	156/153
	Living	Europe	50	37/0

[a] Calibrated years before present (1950 AD). For recent skeletal and living samples, years before 2020 AD. See SOM Tables S4 and S5 for references and SOM S3 for additional information.
[b] Number of data points for body mass/femoral cross-sectional dimensions. For skeletal samples, number of individuals, for living samples, number of sex/population means. Body masses estimated for skeletal samples, measured for living samples.
[c] East Asia defined as Asia east of 90° east longitude.

[2] The exception is some of the Atapuerca specimens, which were sexed based on several criteria (Ruff et al., 2018).

also explored through box plots, scatterplots, and analysis of variance. The Deep Skull femur is particularly highlighted in these comparisons, as the temporally and geographically closest specimen to Trinil 9 and 10 with available cross-sectional properties. SYSTAT (SYSTAT13, 2009) was used for all statistical and graphical analyses.

3. Results

3.1. Age of Trinil 9 and 10

Trinil bone fragments 9 (T-9) and 10 (T-10) were sectioned, polished, and measured by LA-MC-ICPMS for U-series dating (SOM Figs. S1 and S2). Rasters were sampled from the outer (periosteal) to inner (endosteal) surfaces. Trinil 9 did not offer any exploitable data for dating purposes (SOM Table S6). The uranium and thorium concentrations within this fragment were below detection levels for most rasters, and no meaningful isotopic ratios could be calculated for the entire sample. The T-10 samples showed signs of diagenetic processes, with discoloration and cracks within the skeletal tissues (SOM Fig. S1). Many rasters showed the presence of detrital thorium (diffusion of thorium from the sediment into the bone), which required correction of the measured isotopic ratios. Nine rasters provided meaningful isotopic ratios, producing ages of 11.4 ka ± 1.1 to 33.4 ka ± 1.4 (SOM Table S6).

Uranium-series dating is based on the decay of uranium 238 into Thorium 230. Living tissues are usually free of uranium and thorium; therefore, the U-series ages obtained correspond to the migration of the radioisotope into the skeletal tissues after burial and not the death of the individual. The diffusion process can be slow or rapid and can happen early or late in the burial process. Furthermore, the migration can happen in one event, in several waves or continuously, and accumulate over the burial life. Not knowing exactly the uranium diffusion history into the skeletal remains limits the dating accuracy. Therefore, U-series dating provides a minimum age, with the bone being systematically older. Frequently, uranium migrates rapidly (geological time scale) into fossil remains, with preferential pathways in fractures and other decalcified areas. Younger ages in many areas of Trinil 10 can be explained by a heterogeneous uranium diffusion pattern across the tissue. Therefore, the oldest U-series age obtained represents the closest approximation to the true age of the bone. For Trinil 10, this is 33.4 ka ± 1.4. This age corresponds well with the age estimate of 31 ± 6 ka for the terrace in which the fossils were found (see section 2.2. above). Using the minimum U-series date of 32.0 ka and the maximum stratigraphically based date of 37 ka, we arrive at an estimated range of 37–32 ka for the Trinil 9 and 10 specimens.

3.2. Descriptive morphology

The external surface of Trinil 9 is generally well preserved with only minor weathering, most noticeable laterally in the middle region of the shaft (Fig. 1). Proximally the specimen is broken posteriorly and laterally at a level just proximal to the proximal edge of the original lesser trochanter, which is broken off, and distal to the greater trochanter. Anteriorly and medially it extends about 15 mm more proximally and includes a portion of the base of the femoral neck. There is a well-defined gluteal tuberosity. Anteroposterior and M-L breadths 1.5 cm distal to the distal edge of the lesser trochanter base are 23.5 mm and 25.5 mm, respectively, giving a platymeric (A-P/M-L) index of 92, which is relatively round (eurymeric).

The linea aspera is well marked, with a well-developed pilaster (see also Fig. 3 below). Anteroposterior and M-L breadths at 50% of length' (391 mm—see below) are 27.0 mm and 21.4 mm, respectively, giving a pilasteric (A-P/M-L) index of 126. (If a location equivalent to traditional midshaft based on maximum length is used, the index is almost identical.) The distal division of the linea aspera occurs 209 mm from the reconstructed center of the lesser trochanter (distance of Segment 2 in Steele and McKern, 1969). The distal break is irregular and extends a maximum of 63 mm distal to this division. There is a well-defined nutrient foramen at 130 mm from the distal end. The position of minimum M-L breadth (21.0 mm) is at about 150 mm from the distal end, which is proximal to the 50% section (or traditional midshaft based on maximum length).

Trinil 10 is much less well-preserved than Trinil 9. Most of the surface is severely eroded, particularly in the middle and distal regions (Fig. 1). The medial surface is better preserved than the lateral surface in the middle region; this is also evident in cross-sectional contours near midshaft (Fig. 3). The proximal break occurs distal to the lesser trochanter, with a small portion of the medial cortex extending several centimeters proximally, possibly to the distal edge of the neck. Extensive abrasion has removed most surface detail, but the remnants of a linea aspera are visible (Fig. 3). The distal break occurs about 2 cm distal to its apparent division, with a lateral portion of the cortex extending about 2 cm further distally. A crack in the anterior cortex extends about 7 cm proximally from the break. Dimensions taken 110 mm from the most distal extent of the specimen, in a region that appears morphologically to be near the 50% section, are 24.2 mm for both A-P and M-L breadths. These are equivalent to the average 50% location breadth dimensions for Trinil 9, and, factoring in the extensive wear on Trinil 10, indicate that it had a somewhat thicker shaft overall. Given the amount of surface wear and its apparent asymmetry (Fig. 3), it is not possible to assess cross-sectional shape. In terms of general size, the preserved portions of Trinil 10 suggest a reconstructed total length similar to that of Trinil 9. Some anteroposterior bowing of the shaft is apparent in both specimens.

3.3. Bone length and stature reconstruction

Using a Segment 2 length of 209 mm, a mean maximum length estimate for Trinil 9 of 417 mm is obtained when applying the 10 regression equations based on the method of Steele and McKern (1969; see SOM Table S7 for individual results). In using this method, it is implicitly assumed that the proportion of femoral neck length to total maximum length in Trinil 9 would have been equivalent to that of the modern human samples used to develop the regression equations. This assumption is based on other indications that the specimen is morphologically modern (see below), as well as the modern neck length proportions of the earlier Trinil Femur I (Ruff et al., 2015b).

Stature estimates for Trinil 9 using regression equations for five modern samples are shown in Table 5. The femur maximum length ranges for each of the samples are also given, demonstrating that except for the 'Pygmy' sample of Hens et al. (2000), the estimated length of Trinil 9 falls within the range of the reference sample. The mean stature estimate for Trinil 9, rounded to the nearest cm, is 156 cm. All estimates fall between 155.9 and 157.0 cm, i.e., there is little variation despite differences in ethnicity and body size (femur length) ranges.

3.4. Cross-sectional properties

Cross-sectional images extracted from 3-D reconstructions of Trinil 9 and 10 are shown in Figure 3. The length' dimension, used to locate sections, can be calculated from the maximum bone length estimate of Trinil 9 (417 mm) as 391 mm, using the formula presented earlier. Together with the assumption that the 80% section lies 1.5 cm distal to the distal edge of the lesser trochanter (Ruff et al., 2015b), this can be used to locate the 20%, 35%, 50%, and 65%

Table 5
Stature estimates for Trinil 9.

Reference sample	Source[a]	Femur length range (cm)	T9 Stature (cm)
European males	Ruff et al., 2012	38.3–54.3	156.3
Thai males	Gocha et al., 2013	39.1–46.4	157.0
Thai males	Mahakkanukrauh et al., 2011	38.3–50.0	156.5
South African males	Feldesman and Lundy, 1988[b]	39.8–49.9	155.9
'Pygmies'	Hens et al., 2000[c]	34.3–41.0	156.0
Mean			**156**

[a] See SOM Table S1 for individual equations.
[b] Least squares formula. Femur length range estimated from the given standard deviation (SD) as mean ± 2.5 SD, based on the number of SD units that would produce an expected single individual at each end of the range under a normal distribution, with a sample size of 175.
[c] Average of results using inverse (153.9 cm), classical (157.4 cm), reduced major axis (155.6 cm), and major axis (157.2 cm) formulae. Femur length range estimated from the given standard deviation (SD) as mean ± 1.6 SD, based on the number of SD units that would produce an expected single individual at each end of the range under a normal distribution, with a sample size of 19.

sections. The 20% section lies just proximal to the distal end of the specimen. A section close to the presumptive 50% section of Trinil 10 is also shown. This clearly indicates the asymmetric external wear (heavier on the lateral side), as well as the scalloped periosteal surface throughout, except for a smoother portion on the medial-posterior surface. The relatively round subtrochanteric (80%) region and well-developed pilaster of Trinil 9 near midshaft are also evident.

Cross-sectional properties for the five sections of Trinil 9 are given in Table 6. As is typical for human femora (Puymerail et al., 2012; Trinkaus and Ruff, 2012), CA relative to total subperiosteal area (%CA) increases from distal to proximal, reaching a maximum in the 65% section. Relative CA at the 50% location is 70.5%, which is in the lower range for Late Pleistocene anatomically modern *Homo sapiens* (mean ± standard deviation: 79.5 ± 6.5%, range 61%–93%, based on the 66 specimens listed in Tables 3 and 4; see SOM Tables S2 and S3 for individual data). As usual in anatomically modern *H. sapiens*, maximum A-P/M-L bending rigidity (I_x/I_y) occurs in the 50% section, rather than more distally as in archaic *H. sapiens* or *Homo erectus* (Puymerail et al., 2012; Trinkaus and Ruff, 2012; Ruff et al., 2015b). This is consistent with the midshaft or more proximal position of minimum M-L breadth of Trinil 9 noted earlier, which is similar to that of recent humans but again contrasts with archaic *H. sapiens* or *H. erectus*, where it is more distally positioned (Puymerail et al., 2012; Ruff et al., 2015b).

Cross-sectional contours at the 50% location in 17 of the East Asian femora listed in Table 2, including Trinil 9, are shown in Figure 4. Although there is variability within broad temporal groups, femora dated to the late Early or early-middle Middle Pleistocene (i.e., ca. 900–300 ka; Fig. 4, top row) are generally relatively mediolaterally broad compared to those dated to later periods (Fig. 4, bottom two rows). None of the former show evidence for a marked linea aspera or pilaster, while many of the latter do. Some of the variation in morphology within periods is likely due to sexual dimorphism, as shown here for two Tam Hang specimens and explored further below.

These shape differences at midshaft can be quantified using the A-P/M-L bending rigidity ratio (I_x/I_y), which is plotted against time for East Asian, African, and European/West Asian samples in Figure 5. All three regions show a broadly similar temporal pattern: low indices in the Early- to early-Middle Pleistocene (ca. 2000–600 ka), followed by a gradual increase through at least the late Late Pleistocene (ca. 30–12 ka), and then a decrease to recent populations. The precise timing of the latter inflection is difficult to determine in the African sample, given the lack of available Late Pleistocene cross-sectional data. Among the much more densely sampled European/West Asian sample, the decline in the index clearly occurs during the Mesolithic (10.5–5.9 ka). All regions show a decline after the Terminal Pleistocene/early Holocene to very recent samples.

The femora from Trinil follow this same pattern, with lower values of the I_x/I_y index among the late Early to early Middle Pleistocene specimens (Femora II, IV, and V), an increase in the late Middle to early Late Pleistocene Femur I, and a further increase in the late Late Pleistocene Trinil 9. The index for Trinil 9 is relatively high compared to average trends (LOWESS regressions), although not atypical for Late Pleistocene samples, including several East Asian specimens. The Deep Skull femur has a much lower index, but is still well within the range of other Late Pleistocene individuals. The very round ($I_x/I_y \approx 1.0$) midshaft of the Liang Bua 1 femur is also evident.

Another pattern that is apparent in Figure 5 is that although all three regions have broadly similar I_x/I_y values in the Early and Middle Pleistocene, African values are higher than East Asian and European/West Asian values during the Holocene, including both the Late Stone Age sample from South Africa and the very recent sample from East Africa. East Asians and Europeans/West Asians exhibit fairly similar average values throughout. The low position of late Middle Pleistocene/Late Pleistocene archaic *H. sapiens* from Europe/West Asia, i.e., Neandertals, relative to penecontemporaneous specimens from this region, is evident. Tianyuan 1, not included in the calculation of the LOWESS line for East Asians and shown in brackets in the figure, exhibits the highest index of the

Table 6
Cross-sectional diaphyseal properties of Trinil 9 femur.

Location[a]	TA	CA	%CA	I_x	I_y	I_x/I_y	I_{max}	I_{min}	J	Z_x	Z_x	Z_p
20%	623	124	19.9	10581	11869	0.892	11921	10529	22450	766	767	1351
35%	450	220	49.0	14819	9919	1.494	14824	9914	24738	1007	839	1684
50%	422	297	70.5	16594	10345	1.604	16718	10221	26939	1150	906	1871
65%	418	319	76.2	14025	12121	1.157	14126	12020	26146	1133	1038	2059
80%	459	293	64.0	13305	16159	0.823	16507	12957	29464	1084	1169	2081

Abbreviations: TA = total subperiosteal area (mm^2); CA = cortical area (mm^2); %CA = (CA/TA) × 100; I_x and I_y = Antero-posterior (A-P) and medio-lateral (M-L) bending rigidities (mm^4), respectively; I_{max}, I_{min} = maximum and minimum bending rigidities (mm^4); J = torsional and (twice) average bending rigidity (mm^4); Z_x, Z_y = A-P and M-L bending strengths (mm^3), respectively; Z_p = torsional and (twice) average bending strength (mm^3).
[a] Percent of bone length from distal end (see text, sections 2.4 and 2.5).

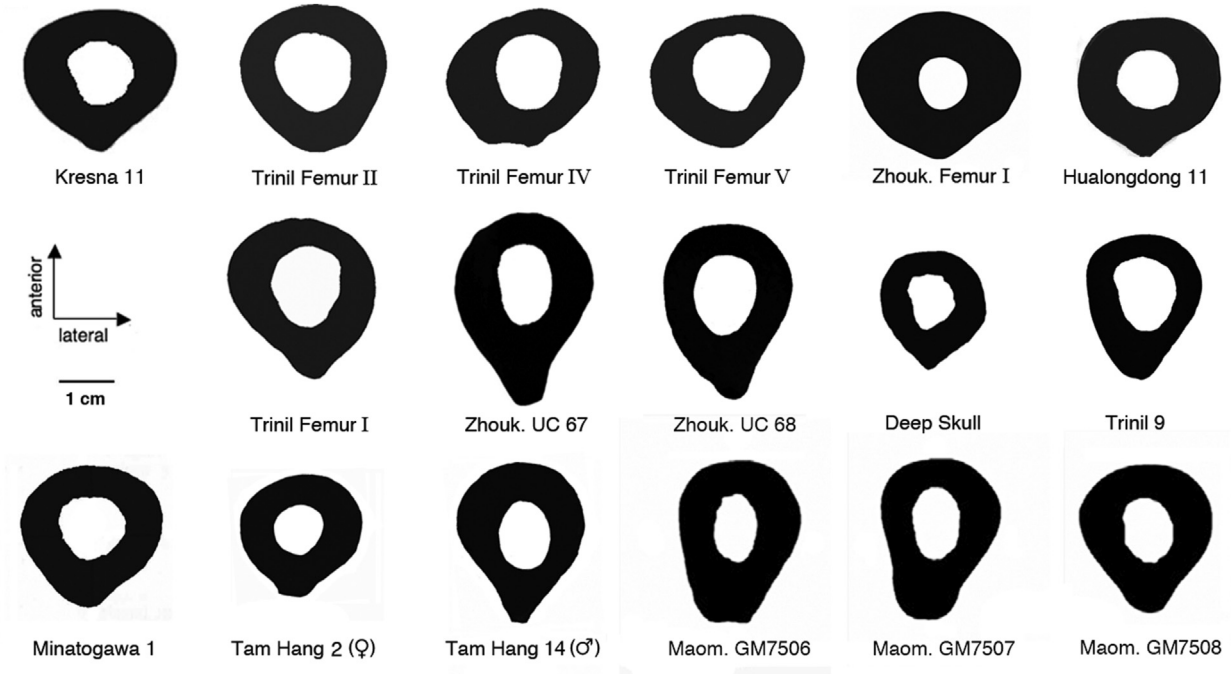

Figure 4. Femoral midshaft (50% location) cross sections of representative East Asian Pleistocene specimens. Specimens arranged in chronological order from top left to lower right. Top row: late Early Pleistocene-middle Middle Pleistocene (ca. 900–300 ka); middle row: late Middle Pleistocene-early Late Pleistocene (140–26 ka); bottom row: late Late Pleistocene (20–14 ka). Zhouk.: Zhoukoudian; Maom.: Maomaodong. See Table 2 and SOM Table S2 for details on individual specimens. Sources of images: Kresna 11: Puymerail et al. (2012); Trinil Femora I, II, IV, V: Ruff et al. (2016); Zhoukoudian Femur I: Weidenreich (1941); Hualongdong 11: Xing et al. (2021); Zhoukoudian UC 67, 68: Weidenreich (1941) and present study (see SOM S1); Deep Skull: Curnoe et al. (2019); Trinil 9: present study; Minatogawa 1: Kimura and Takahashi (1992); Tam Hang 2, 4: L.L. Shackelford (pers. comm., 3/11/20); Maomaodong GM7506, 7507, 7508: Wei et al. (2021).

entire sample. The two Zhoukoudian Upper Cave and two of the three Maomaodong specimens show the next highest values among Late Pleistocene East Asian specimens (also see Fig. 4).

Temporal trends in the I_x/I_y index by sex are shown in Figure 6. Throughout the Pleistocene and early Holocene, males always have higher indices on average than females. However, there is no difference between the sexes in any of the recent samples (also see below). Trinil 9, with its high index, falls above the average male trend line but well within the male distribution, and above almost all (96%) of females. The Deep Skull femur falls directly on the average female trend line.

Because the trends shown in Figure 6 could potentially be influenced by geographic differences and sex bias in representation between regions, comparisons of femoral midshaft I_x/I_y between the sexes within narrow temporally and geographically defined groups, or when possible, specific sites, were also carried out, with results given in Figure 7. In every comparison within samples, except for very recent populations, males show greater average values of the index than females. This is true of all three regions, and samples spanning the Middle Pleistocene through the early Holocene. Furthermore, it is characteristic of samples that on the whole vary greatly in the index, e.g., Neandertals and South African Late Stone Age samples. A multiple analysis of variance among pre-late Holocene samples with group and sex as predictors shows a highly significant effect of both variables on femoral midshaft I_x/I_y ($p < 0.0001$). Thus, differences in average shape between regions or periods do not affect sexual dimorphism in shape. A lack of sexual dimorphism among modern (20th century) populations is also characteristic of all three regions, despite variation in overall values of the index between regions (i.e., modern Africans have higher indices than Europeans or Japanese). Temporal changes within regions, in both sexes, are also evident, supporting results for the sex-combined samples shown in Figure 5.

Trinil 9 has an I_x/I_y value that is most similar to those of males from the Skhul-Qafzeh and South African Late Stone Age samples. It also overlaps broadly with European Late Upper Paleolithic and Jomon males, and is close to the Tam Hang male. The Deep Skull femur overlaps broadly with females from several samples, including Jomon and Tam Hang, as well as some male samples, the latter from groups with overall low indices (e.g., Neandertals, modern samples). The contrast in cross-sectional shape (as well as overall size) between Trinil 9 and the Deep Skull femur is very similar to that between a male and female from Tam Hang (Fig. 4).

3.5. Body mass

Body mass estimation equations using femoral 50% CA, and CA and femoral maximum length, based on 69 Pleistocene femora with articular estimates of body mass (67 for CA and length), are given in Table 7. Percent standard errors of estimate and average absolute prediction errors are relatively low: 9–11% and 7–8%, respectively. (It should be recognized that true prediction errors will be higher than this, because body mass was itself estimated in the reference sample.) The addition of bone length as a predictor reduces estimation errors, so this technique was used whenever possible. Among the 192 Pleistocene specimens with estimated body masses (Tables 3 and 4), 145 are estimated from articular size (of the lower limb except for Tianyuan 1, estimated from its distal humerus), 20 from CA and femoral length, and 27 from CA alone (see SOM Tables S2 and S3 for details). Body masses of all of the Holocene samples are estimated from lower limb articular size.

The body mass of Trinil 9 is estimated from its 50% section CA and the estimated maximum length is 55.4 kg. Body mass estimated from CA alone is 51.5 kg. Because of the smaller estimation errors of the combined formula, 55.4 kg is used in all subsequent analyses. An accurate body mass cannot be estimated for Trinil 10,

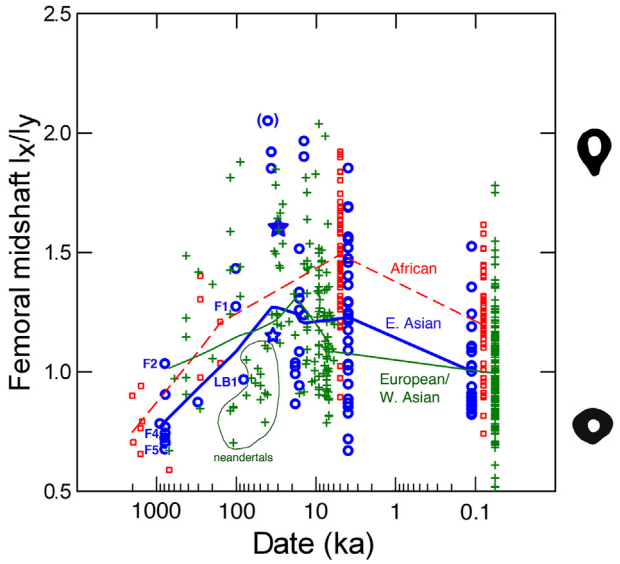

Figure 5. Temporal trends in femoral midshaft (50% location) anteroposterior to mediolateral bending rigidity in East Asian, sub-Saharan African, and European/West Asian specimens, fit with LOWESS regression lines. The x-axis scale is in logarithmic units. Representative cross-sectional shapes associated with specific bending rigidity ratios shown to right. East Asians: blue circles and heavy solid line; Africans: red squares and dashed line; European/West Asians: green crosses and thin solid line. Solid blue star: Trinil 9; open blue star: Deep Skull (Niah Cave) specimen. F1, F2, F4, F5: Trinil Femora I, II, IV, V. LB1: Luang Bua 1 specimen. European/West Asian Neandertals outlined. See Tables 2–4 and SOM Tables S2–4 for composition of samples. Tianyuan 1 indicated within parentheses (value derived from section properties corrected for obvious pathological deposits, provided by S. Xing), not used in calculating East Asian trend line. In all three regions, cross-sectional shape is relatively mediolaterally expanded in Early and early Middle Pleistocene specimens, becomes more anteroposteriorly oriented in the later Middle Pleistocene and Late Pleistocene, and then becomes rounder among very recent populations. The Pleistocene trend is apparent within the site of Trinil itself.

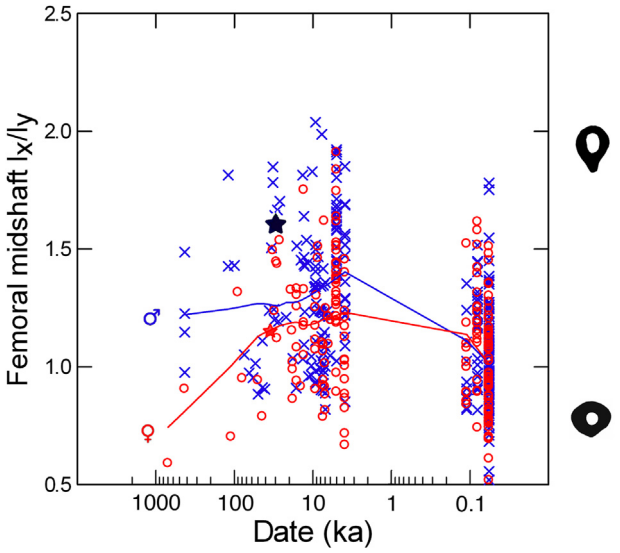

Figure 6. Temporal trends in femoral midshaft (50% location) anteroposterior to mediolateral bending rigidity, separately by sex. Males: blue x's; females: red circles. Trend lines within sex fit with LOWESS regressions. The x-axis scale is in logarithmic units. Representative cross-sectional shapes associated with specific bending rigidity ratios shown to right. Black solid star: Trinil 9; red solid star: Deep Skull (Niah Cave) specimen. See Tables 2–4 and SOM Tables S2–4 for composition of samples. Males show consistently greater anteroposterior reinforcement of the shaft on average throughout the Pleistocene and early Holocene, until very recent populations where the sexes are indistinguishable. The Trinil 9 and Deep Skull specimens fall near the middle of the distributions for Late Pleistocene males and females, respectively.

given its state of preservation. It has a measured CA of 280 mm^2, which produces a body mass estimate of 50.1 kg; therefore, its actual estimated body mass with a restored cortex would have been larger than this.

Temporal trends in estimated body mass in the three regional groups are shown in Figure 8. Average body masses in the Early and early Middle Pleistocene are similar in all three regions, decline during the Middle and/or Late Pleistocene, and then remain relatively constant during the Holocene. The timing of the decline in body mass varies somewhat between regions, with African and East Asian samples showing a steady decrease (on average) through the Middle and Late Pleistocene, and the European/West Asian sample only decreasing during the later Late Pleistocene (ca. 30–11 ka). However, the apparent decline through the Middle Pleistocene among Africans is heavily influenced by the inclusion of five femora of *Homo naledi*, which has been shown to be quite small-bodied for Pleistocene *Homo* (Garvin et al., 2017). Thus, we also calculated a LOWESS line through the African sample excluding *H. naledi*, and plot this in Figure 8. If *H. naledi* is excluded, the general temporal trend line for Africans does not begin declining until the Late Pleistocene, and is consequently similar to that of Europeans/West Asians throughout the Middle Pleistocene. Regardless, by the later Late Pleistocene and Holocene, including very recent populations, Europeans/West Asians are larger in body mass than East Asians and Africans, which are similar to each other. Average regional body masses for the very recent skeletal samples and living samples, the latter including a wide geographical range (see above and SOM Table S5 and SOM S3), are similar, indicating that the lower body masses for very recent populations are not biased by the specific skeletal samples included. There is, however, a slight indication of an increase in the most recent living European samples, reflecting recent secular trends in this region (Ruff, 2018). The slight upward shift in East Asian body masses in the large Holocene (3.9 ka) Jomon sample in Figure 8 may be climatically related (see Discussion).

Trinil 9 falls close to the general trend line for Late Pleistocene East Asians, whereas the Deep Skull femur falls well below it, but within the range of several other East Asian specimens (also see Figs. 9 and 10). Following the general East Asian temporal trend, the three early Trinil femora (Femora II, IV, and V) and the late Middle to early Late Pleistocene Trinil Femur I are larger than Trinil 9 (Femur V just barely), and similar in size to early femora from Zhoukoudian and Kresna. The Wajak femur falls in the larger size range for Late Pleistocene East Asian specimens, slightly higher than Trinil Femur I. The two largest East Asian Pleistocene specimens are Jinnuishan 1 (260 ka) and Tianyuan 1 (40 ka). The very small body mass of the Liang Bua specimen is apparent. Inclusion of this specimen in the East Asian sample has no discernable effect on the general trend line for this group, however.

Temporal trends in body mass by sex are shown in Figure 9. As expected, males are consistently larger than females throughout all periods. When grouped in this way (i.e., averaged across regions), each sex shows a slight decline in body mass through the Middle Pleistocene, followed by a rapid decline in the Late Pleistocene, then a leveling off through very recent samples. Trinil 9 falls just below the average body mass of females, and the Deep Skull femur is in the smaller range for females.

Body mass estimates for Late Pleistocene East Asian males, females, and individuals of indeterminate sex, by site, are shown in Figure 10. Trinil 9 is smaller than two males from Minatogawa and Tam Hang, but larger than the Liujiang male specimen, and overlaps with the largest female from Tam Hang. The Deep Skull femur falls within a cluster of females from Minatogawa and Tam Hang. The

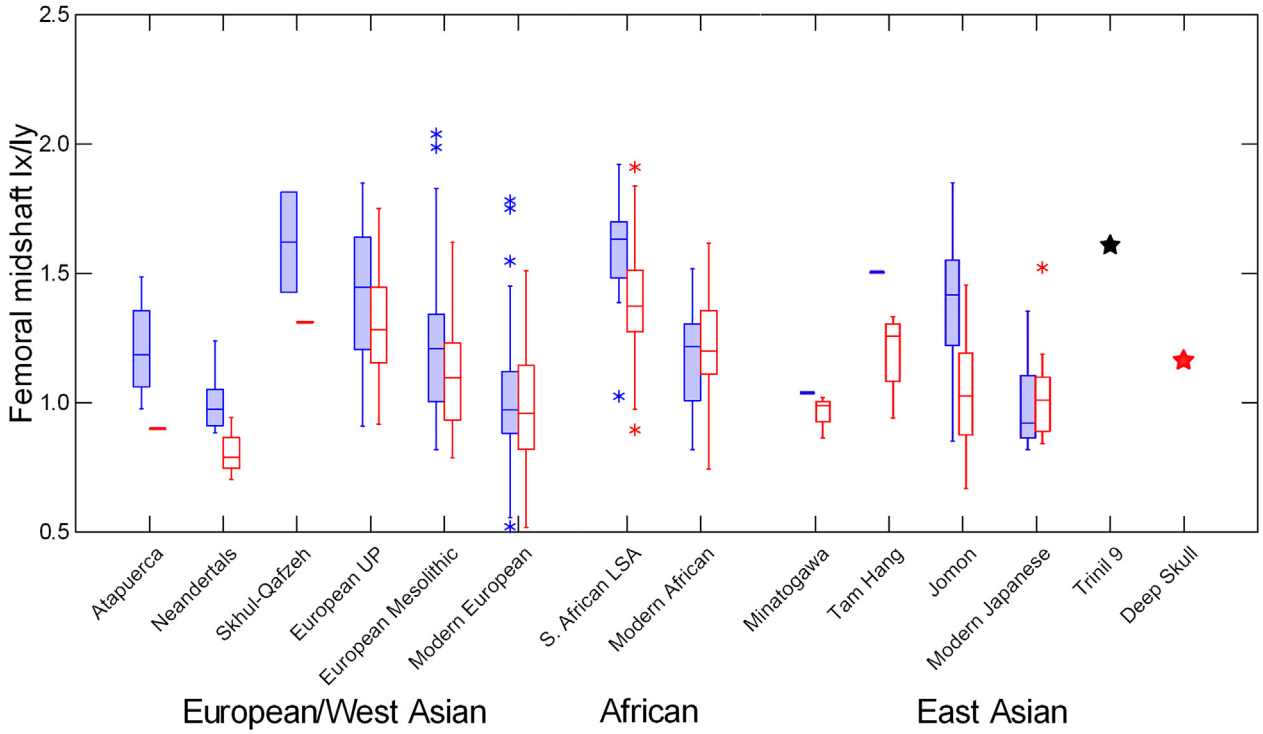

Figure 7. Box plots of femoral midshaft (50% location) anteroposterior to mediolateral bending rigidity in males and females within narrowly defined temporal/geographic groups, or single sites, arranged chronologically within three major geographic regions. Males: solid blue boxes; females: open red boxes. Black solid star: Trinil 9; red solid star: Deep Skull (Niah Cave) specimen. UP = Upper Paleolithic; LSA = Late Stone Age. See Tables 2–4 and SOM Tables S2–4 for composition of samples. Modern samples are recent skeletal samples. In all Pleistocene and early Holocene comparisons, males show relatively greater anteroposterior rigidity than females on average, except for modern populations where they are equivalent. The difference between the Trinil 9 and Deep Skull femora is similar to that between males and females of the Tam Hang and Jomon skeletal samples.

Table 7
Body mass estimation equations.

Equation[a]	*n*	r	SEE[b]	%SEE[c]	|%PE|[d]
Body mass = CA × 0.0797 + 27.8	69	0.782	7.0	10.9%	8.5%
Body mass = CA × 0.0448 + FL × 0.1136−5.3	67	0.832	6.0	9.3%	7.2%

[a] CA = cortical area at femoral 50% section (mm^2); FL = femoral maximum length (mm); body mass in kg.
[b] Standard error of estimate (kg).
[c] Percent standard error of estimate.
[d] Absolute value of percent prediction error.

specimens of indeterminate sex, including Trinil Femur I, fall within or above the range of males, whereas Liang Bua is again much smaller than any other specimen, although within 7 kg (18%) of one female from Tam Hang.

4. Discussion

4.1. General characteristics

The general morphology of Trinil 9 is consistent with that of anatomically modern *H. sapiens* in both East Asia and worldwide, with none of the features characteristic of archaic *H. sapiens* and/or *H. erectus* (Weidenreich, 1941; Day, 1984, 1986; Ruff, 1995; Trinkaus and Ruff, 2012): it is not platymeric (relatively M-L expanded) proximally; the position of minimum M-L breadth is located near or proximal to rather than distal to midshaft; it has a high A-P/M-L bending rigidity ratio in the middle region of the diaphysis, with a well-marked linea aspera and pilaster; and it does not have relatively thick cortices. Relative M-L expansion of the proximal femoral diaphysis has been postulated to be related to a relatively long femoral neck in *H. erectus* and earlier '*erectus*-like' *Homo*, increasing M-L bending loads on the proximal femoral shaft (Ruff, 1995). Such a loading pattern would also contribute to a rounder femoral midshaft region and a less apparent linea aspera and pilaster, although these may also be affected by general body shape differences as well as behavior (see below). The extreme wear on Trinil 10 precludes assessment of these characteristics, but it does show evidence of a linea aspera, and no evidence for M-L broadening of the proximal shaft.

In contrast, Trinil Femora II–V, from the late Early to early Middle Pleistocene, show a morphology more consistent with that of *H. erectus* worldwide (present results; see also Ruff et al., 2015b). Trinil Femur I aligns morphologically with Late Pleistocene anatomically modern humans (AMH), consistent with its relatively short neck, although it is less extreme in this regard than Trinil 9. This could be related to differences in body shape or behavior between the two specimens, or simply represent the range of morphologies characteristic of Late Pleistocene AMH. In any event, the temporal sequence of femoral morphologies at Trinil parallels that seen more generally within Pleistocene *Homo*, and is the only example to date where this can be assessed within a single site.

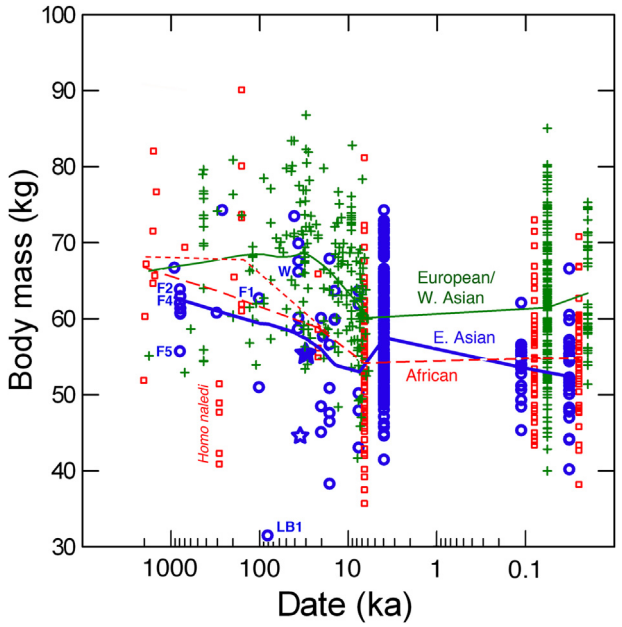

Figure 8. Temporal trends in estimated body mass in East Asian, sub-Saharan African, and European/West Asian specimens, fit with LOWESS regression lines. The x-axis scale is in logarithmic units. East Asians: blue circles and heavy solid line; Africans: red squares and dashed line (all specimens) and dotted line (excluding *H. naledi* specimens); European/West Asians: green crosses and thin solid line. Solid blue star: Trinil 9; open blue star: Deep Skull (Niah Cave) specimen. F1, F2, F4, F5: Trinil Femora I, II, IV, V. W: Wajak specimen. LB1: Luang Bua 1 specimen. *Homo naledi* specimens indicated. See Tables 2–4 and SOM Tables S2–5 for composition of samples. Three most recent groups are sex/population means for living samples (see Table 4 and SOM Table S5), slightly offset in time to avoid overlap. Body mass declines between the Early and early Middle Pleistocene to the early Holocene, and is larger on average in European/West Asian specimens from the Late Pleistocene through recent populations. Trinil 9 and Deep Skull are both relatively small-bodied, but fall well within the range for East Asian Late Pleistocene specimens.

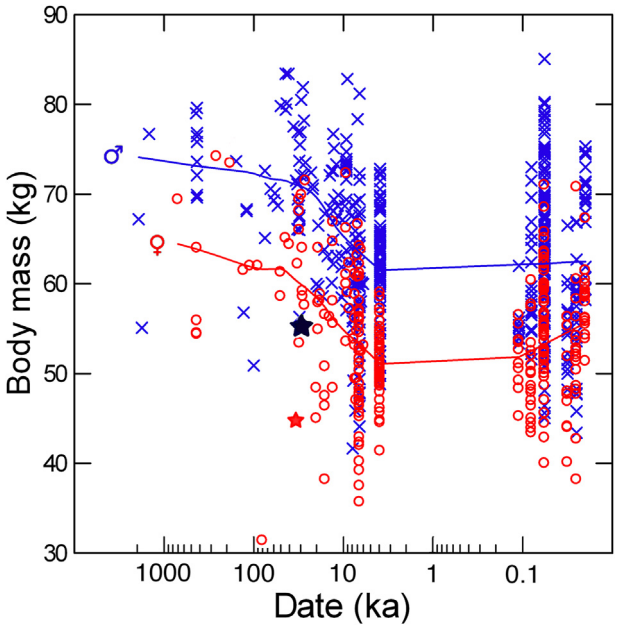

Figure 9. Temporal trends in estimated body mass, by sex. Males: blue x's; females: red circles. Trend lines within sex fit with LOWESS regressions. The x-axis scale is in logarithmic units. Black solid star: Trinil 9; red solid star: Deep Skull (Niah Cave) specimen. See Tables 2–4 and SOM Tables S2–5 for composition of samples. Three most recent groups are sex/population means for living samples (see Table 4 and SOM Table S5), slightly offset in time to avoid overlap. Males and females show very similar temporal trends in body mass, with a slow decline in the Middle Pleistocene and an accelerating decline in the Late Pleistocene. The difference in body mass between Trinil 9 and Deep Skull is similar to the average difference between males and females.

A partial proximal femur from the Terminal Pleistocene (14.3–13.6 ka) site of Maludong, in Southwest China, has been claimed to possess archaic features similar to those of Early Pleistocene *Homo* (Curnoe et al., 2015). If true, this could have important implications regarding the retention of nonmodern postcranial morphology and temporal overlap between archaic and anatomically modern *Homo* in East Asia (Curnoe et al., 2015; Wei et al., 2020, 2021). However, as described in more detail in SOM S4, we find this interpretation of the Maludong specimen to be unconvincing, for several reasons. These include lack of data (preservation of the proximal end of the specimen is insufficient to accurately estimate femoral neck length); questionable orientation of the specimen relative to A-P and M-L axes, which affects assessment of the position of the lesser trochanter as well cross-sectional diaphyseal dimensions; incorrect identification of midshaft, based on a total length estimate that appears to be too short, which also affects cross-sectional diaphyseal dimensions; and an inappropriate method for standardizing dimensions for body size. Thus, in our opinion, this specimen provides little or no evidence for the retention of archaic postcranial features in a 'relic' mainland East Asian Late Pleistocene population (contra Curnoe et al., 2015).

Postcrania of other small-bodied, island endemic hominins in Southeast Asia, including *Homo luzonensis* and *Homo floresiensis*, do show clear archaic features (Brown et al., 2004; Morwood et al., 2005; Tocheri et al., 2007; Jungers et al., 2009a, b; Détroit et al., 2019). A detailed consideration of the Liang Bua 1 *H. floresiensis* femur is beyond the scope of this study; however, it can be noted that, as in previous descriptions (Brown et al., 2004; Jungers et al., 2009b), we found its midshaft region to be very round, that is, to

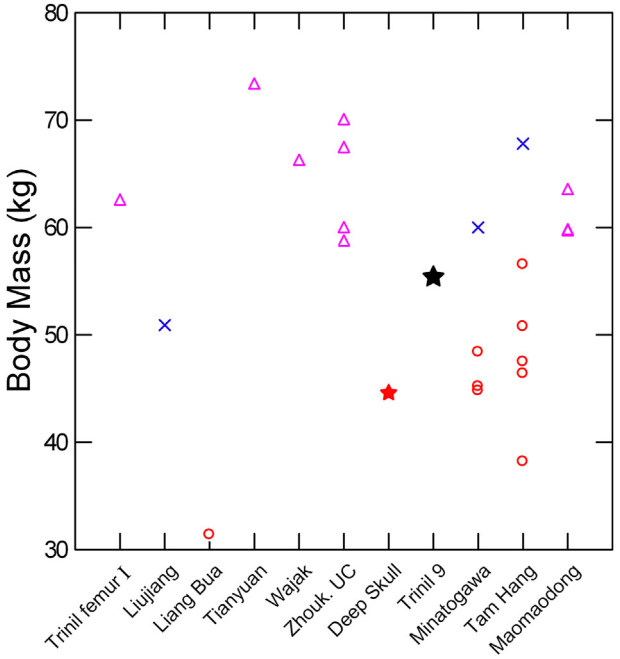

Figure 10. Estimated body mass in late Middle-Late Pleistocene East Asian specimens, arranged chronologically from left to right. Males: blue x's; females: red circles; not sexed: purple triangles. Black solid star: Trinil 9; red solid star: Deep Skull (Niah Cave) specimen. Zhouk. UC = Zhoukoudian Upper Cave. See Table 2 for complete list of specimens. Both Trinil 9 and Deep Skull fall within the range of values for males and females, respectively.

have an I_x/I_y ratio close to 1.0. In this regard, it resembles not only Neandertals (Jungers et al., 2009b) but also several other Middle and Late Pleistocene femora from East Asia. The implications of small body size in both *H. luzonensis* and *H. floresiensis* in an East Asian context are discussed in the next section.

Based on its midshaft cross-sectional shape, we infer that Trinil 9 was very likely male. Anteroposterior/M-L bending rigidity of the middle region of the femoral diaphysis is consistently higher on average in males in all our Pleistocene and early Holocene samples. Trinil 9 falls within the higher range for Pleistocene males, and above almost all females. It fits comfortably within the male distributions of values for several other Pleistocene and early Holocene samples from East Asia, Africa, and Europe/West Asia. The Deep Skull femur, which is very likely female based on its association with the Deep Skull cranium (Curnoe et al., 2016, 2021), has a much lower A-P/M-L bending rigidity index. The contrast in cross-sectional shape between Trinil 9 and the Deep Skull femur is very similar to the degree of sexual dimorphism in this parameter observed within the Late Pleistocene site of Tam Hang and the early Holocene Jomon sample. As discussed further below (section 4.3.), the underlying explanation for the consistent sex difference in femoral shape, before very recent humans, is likely to be primarily behavioral.

4.2. Body size

The estimated body mass of Trinil 9 (55.4 kg) is small for a male when considered in a worldwide Late Pleistocene context. However, it is 24% larger than the estimated body mass of the Deep Skull individual (44.6 kg), which is very likely to be female. The Wajak femur, representing another Southeast Asian penecontemporaneous individual, is larger (65.4 kg), as is the terminal Middle to early Late Pleistocene Trinil Femur I individual (62.6 kg). Détroit and coworkers (Détroit et al., 2004, 2013; Corny et al., 2016) have commented on the great dispersion in size and robusticity represented in the Late Pleistocene (47–16 ka) Tabon Cave site (Palawan, Philippines), with some cranial material showing similarities to the very large and robust Wajak 2 mandible and other specimens to the much smaller and more gracile Deep Skull cranium. They felt that the range of variation exceeded that to be expected from sexual dimorphism within a single population, and suggested instead the possible existence of two morphologically distinct populations at the site, with the smaller-bodied population linked to the Niah Cave (Deep Skull) individual. [Palawan was likely separated by water from Sundaland, including Niah Cave, during the Late Pleistocene (Voris, 2000), but was very close to it, with a very similar fauna, unlike the considerably more endemic environment in more eastern regions of the Philippines, including Luzon (Détroit et al., 2013)]. If this is true, then Trinil 9 could represent a male of such a small-bodied population, with Wajak and Trinil Femur I belonging to a larger-bodied population, or possibly representing other males of the small-bodied population. As discussed previously (Curnoe et al., 2021), there is nothing in the morphology of the Deep Skull femur to associate it specifically with Southeast Asian 'Negrito' populations, and the same is true for the Trinil 9 femur, although the possibility of a historical/genetic relationship between small-bodied Pleistocene and modern populations in the region cannot be ruled out (Détroit et al., 2013; Curnoe et al., 2016).

Evidence for even smaller-bodied humans has been found on the more geographically isolated islands of Southeast Asia, including Luzon, Philippines (*H. luzonensis*; Mijares et al., 2010; Détroit et al., 2019), and Flores (*H. floresiensis*; Brown et al., 2004; Morwood et al., 2005; Jungers et al., 2009b). Our body mass estimate for the LB1 individual from Liang Bua, Flores, based on femoral head breadth, is 31.4 kg, considerably smaller than our mean for Mbuti females (38.2 kg), the smallest living humans. The latter matches the estimated body mass of our smallest Pleistocene individual, a female from Tam Hang, and is close to the smallest values estimated from femoral head size for two 'Negrito' populations: the Aeta, from Luzon (Curnoe et al., 2021), and Andaman Islanders (Stock, 2013, pers. comm., 5/19/21). Our estimate for LB1 falls within the range of values cited by Brown et al. (2004), 16–36 kg, and is relatively close to their estimate based on the estimated stature of LB1 and stature/body mass proportions of adult African 'Pygmies' (28.7 kg), and also to that of Jungers et al. (2009a: SI Table 2; 32.5 kg), based on femoral head diameter and equations in McHenry (1992). Given that an adult tibia from Liang Bua, LB8/1, is considerably smaller than the corresponding element of LB1 (Morwood et al., 2005; Jungers et al., 2009b; also see van den Bergh et al., 2016a), it is clear that extremely small body size was characteristic of this taxon. No body masses have been estimated for the more limited postcranial remains available for *H. luzonensis*, but preserved dental and postcranial elements are similar, if not smaller, in size than corresponding elements in *H. floresiensis* (Mijares et al., 2010; Détroit et al., 2019), suggesting a similar body size. The fact that no Pleistocene individual from what was then mainland Southeast Asia (including Sundaland) has been found with a body mass in this range emphasizes the highly endemic nature of both taxa, which may have developed in situ since the early Middle Pleistocene or earlier (Brumm et al., 2010; van den Bergh et al., 2016a; Ingicco et al., 2018).

Climatic adaptation may also have played a role in body size distributions observed in Pleistocene and modern East Asia. Bergmann's Rule (Bergmann, 1847)—that within endothermic species spanning a wide geographic range, larger-bodied populations will be associated with colder climates and smaller-bodied populations with warmer climates—has been found to apply in general to modern humans (Roberts, 1953, 1978; Ruff, 1994; Foster and Collard, 2013). The two largest individuals (73–74 kg) in our East Asian Pleistocene sample—Tianyuan 1 and Jinnuishan 1—are both from northern latitudes. As Jinnuishan 1 is female (Rosenberg et al., 1999), this suggests the likelihood of even larger body masses for late Middle Pleistocene northern Asian males. A few of the Holocene Jomon individuals reach this body mass range, but this sample is also from a mid-higher latitude (34–44° N.; Temple, 2008), higher than our preceding Terminal Pleistocene and early Holocene samples (Tam Hang, Maomaodong, and Cau Giat). This may explain the slight upward shift of East Asian body mass values that we found in the corresponding period for the Jomon sample (3.9 ka). Among living East Asian populations in our sample, the largest sex/population average body mass is for Mongolian males (66.5 kg), with small-bodied males (<56 kg) and females (<49 kg) all limited to tropical and subtropical regions ($\leq$24° N. latitude). A more formal analysis of climatic effects on body size variation during the Pleistocene would include estimates of actual paleoclimatic conditions (e.g., Will et al., 2021). The interaction of population history and climatic adaptation on body size distributions in East Asia must also be considered (Dennell et al., 2020). However, on a general level, the tropical and subtropical climatic conditions of Southeast Asia may have contributed to the presence of small-bodied populations/taxa in this region, including those represented by Trinil 9 and the Deep Skull femur.

Climatic adaptation may also at least partly explain broader patterns of variation in body size observed in our worldwide comparisons. From at least the beginning of the Late Pleistocene through to the present, populations from East Asia and sub-Saharan Africa average smaller body masses than those from Europe/West Asia. As the latter are from systematically higher latitudes (with a few East Asian exceptions, including those noted earlier), the

difference in average body size also conforms to the expectations of Bergmann's Rule. Thus, regional differences in body size since the Late Pleistocene may be largely attributable to environmental effects (also see Shackelford, 2007). The possible effects of systematic differences in nutritional levels between regions should also be considered here (Black et al., 2013; Akseer et al., 2017), but the fact that this pattern is also present before the last few centuries suggests that recent disparities of this kind do not explain all the observed regional variations. The very wide range of body mass values within regions, particularly in Africa, should also be appreciated. In every period before very recent populations where there are sufficient data for comparisons—in the Early Pleistocene, Middle Pleistocene, and early Holocene—Africa has a greater range of body mass values than Europe/West Asia or East Asia (this does not include the endemically dwarfed Liang Bua specimen). Whether this reflects increased competition for resources (Garvin et al., 2017), adaptations to local environmental conditions in semi-isolated populations (Scerri et al., 2018), and/or greater genetic diversity among African populations (Campbell and Tishkoff, 2008), are topics worthy of further exploration.

The estimated stature of Trinil 9 of 156 cm is not too far below the mean for 18 different samplings of living rural Indonesian men carried out in the early-mid-20th century (159.3 cm, range of sample means 156.5–163.5 cm; Bailey, 1962). The body mass index (BMI) of Trinil 9, calculated from its estimated body mass and stature [BMI = (body mass (kg)/stature^2 (m)) × 100], is 22.8 kg/m^2, which is somewhat higher than our average for modern tropical-subtropical populations (<30° latitude, 20.8 kg/m^2; SOM Table S5). It is also similar to that of very recent urban Indonesian males (22.2 kg/m^2; Chuan et al., 2010).

We would like to add one final word regarding the application of the new body mass estimation methods developed here. As the Trinil 9 femur lacked articulations, its body mass was estimated from midshaft CA and estimated length, using a Pleistocene *Homo* reference sample. Because cortical diaphyseal morphology is developmentally responsive to mechanical loadings during life, use of such a methodology presumes that loadings due to factors other than body mass per se do not vary systematically between the reference sample and target specimen. As noted earlier, this assumption appears reasonable for Pleistocene *Homo*, in general. However, there is evidence that non-*Homo* taxa have stronger limb bones relative to body size, due perhaps to greater overall muscular loadings (Ruff et al., 2016). Thus, it would not be appropriate to apply the present equations to such taxa. Differences in locomotor behavior that could affect lower limb loadings, i.e., increased arboreality and/or altered terrestrial bipedalism in non-*Homo* taxa as well as *Homo habilis* sensu stricto (Lovejoy et al., 2009; Ruff, 2009; Zipfel et al., 2011; Churchill et al., 2013; Ruff et al., 2016), also argue against application of equations developed from a fully bipedal *Homo* reference sample. Given some evidence from the upper limb that *H. naledi* retained significant arboreal capabilities (Kivell et al., 2015; Feuerriegel et al., 2017), this might also suggest caution in applying the present estimation equations, although lower limb bones of this taxon appear to be essentially modern in most respects (Harcourt-Smith et al., 2015; Marchi et al., 2017). Application of any technique that includes diaphyseal cortical geometry as a predictor will increase estimation error due to inevitable individual variation in non-body mass-related factors such as activity level (Ruff et al., 2018). We attempted to minimize such errors by using an appropriate reference sample and a geometrical parameter that may be less influenced by bending and torsional loadings generated by vigorous activity, but the limitations of this method should also be recognized when applying it to any paleontological specimen.

4.3. Body shape and behavior

Both body shape and behavior have been implicated as factors influencing cross-sectional diaphyseal shape of the lower limb bones (for a review, see Ruff and Larsen, 2014). Body (pelvic) breadth is negatively correlated with femoral midshaft A-P/M-L bending rigidity (I_x/I_y), i.e., wider bodies are correlated with more M-L reinforced shafts (Weaver, 2003; Shaw and Stock, 2011), as predicted theoretically (Ruff, 1995).[3] In addition, longer femoral necks are associated with increased M-L bending strength of the femoral shaft, again as expected based on theoretical models (Ruff, 1995). In contrast, greater terrestrial mobility is associated with higher femoral midshaft A-P/M-L bending rigidity (Ruff, 1987; Stock, 2006). This is likely due to increases in relative anteroposterior bending of the lower limb bones—particularly in regions near the knee—with increased mobility (Ruff, 1987, 2005), an effect that is magnified in areas with rougher terrain (Holt and Whittey, 2019).

Figure 11 shows a simple summary of these contrasting effects. The combination of effects suggests that the highest I_x/I_y values will be found in populations or taxa with short femoral necks, narrow bodies, and high mobility, whereas the lowest I_x/I_y values will be associated with long femoral necks, wide bodies, and low mobility. Populations or taxa with different combinations of morphology and behavior should exhibit mixed or intermediate effects on cross-sectional shape, e.g., a narrow body combined with lower mobility should result in a moderate I_x/I_y value.

These predictions can be used to interpret observed temporal and regional differences in cross-sectional shape in our samples, including Trinil 9. Where it can be evaluated, a relatively long femoral neck is characteristic of all Early Pleistocene and early Middle Pleistocene *Homo* (Ward et al., 2015; Ruff et al., 2015b). This is likely part of a functional complex that includes a relatively wide pelvis as well (Ruff, 1995). Thus, as predicted, femoral specimens from this time range exhibit low I_x/I_y values (also see Trinkaus and Ruff, 2012; Ward et al., 2015). In addition to East African specimens dating to 2035–700 ka, this includes East Asian specimens from Kresna, Trinil, and Zhoukoudian (900–770 ka) as well as our earliest European/West Asian specimens (Gesher Benot Ya'aqov and Ain Maarouf, 700–600 ka). Femoral midshaft I_x/I_y values then increase during the later Middle Pleistocene and Late Pleistocene, as femoral neck length assumes more modern proportions (Weaver, 2003; Carretero et al., 2012; Ruff et al., 2015b). Neandertals are a partial exception, retaining relatively low I_x/I_y values, probably as a result of their 'hyperpolar' (very wide) body form (Weaver, 2003). Peak I_x/I_y values are reached in the late Late Pleistocene or early Holocene in all three major regions, then decline in very recent populations. As there is no evidence that fundamental body shape within regions changed systematically during the Terminal Pleistocene/Holocene, the recent decline in the index is best attributed to a decline in mobility, first manifested in the Mesolithic and continuing through the introduction of food production and a more sedentary lifestyle during the Holocene (Ruff et al., 2015a; Holt et al., 2018). African populations have systematically higher indices during the Holocene because of their

[3] This concept has been critiqued (Pearson et al., 2014). However, that study examined correlations between femoral midshaft maximum/minimum bending rigidity (I_{max}/I_{min}) and pelvic breadth, not A-P/M-L bending rigidity and pelvic breadth or relative breadth. The two measures of femoral midshaft shape are not equivalent, i.e., the direction of maximum bending rigidity of the femoral midshaft departs significantly from anteroposterior (Ruff and Hayes, 1983), and may even more closely approximate mediolateral (see Fig. 4). Thus, analyses of I_{max}/I_{min} cannot be used to test predicted associations between midshaft femoral and body shape.

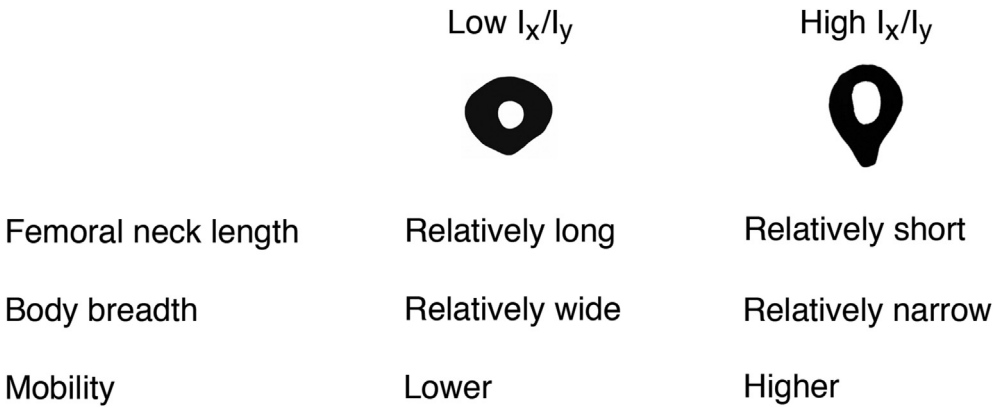

Figure 11. Theoretical model relating variation in femoral midshaft shape (I_x/I_y, anteroposterior/mediolateral bending rigidity) to femoral neck length, body shape, and mobility.

relatively narrow bodies (Ruff, 1994). Our South African Late Stone Age sample, with a very high I_x/I_y index, is characterized by a very narrow pelvis, particularly relative to lower limb length (Stock, 2013). Their cross-sectional shape is exactly what would be predicted for a narrow-bodied, mobile (Stock and Pfeiffer, 2001) population (Fig. 11).

Trinil 9 conforms well to this temporal pattern, with a high I_x/I_y value that falls near the middle of the distribution for anatomically modern Late Pleistocene males. Among other East Asian Late Pleistocene specimens, it falls below the values for the two Zhoukoudian Upper Cave femora and two of the femora from Maomaodong, and somewhat above Trinil Femur 1, Liujiang 1, and the Tam Hang male. Barker et al.'s (2007) investigation of Niah Cave, the source of the Deep Skull femur, sheds light on the paleoecology and subsistence strategy of the inhabitants of another inland Southeast Asian site that is nearly contemporaneous with the Trinil 9 specimen. The Niah Cave inhabitants combined hunting of a range of terrestrial, terrestrial-arboreal, and aquatic vertebrates with procurement of a variety of botanical resources. They were mobile, exploiting several different habitats within the general region of the cave, including tropical forest, swamp, open woodland, scrub, and the shores of rivers and lakes. Stone sources for tools found in the cave ranged up to almost 50 km away. While microenvironmental conditions varied across Sundaland during the Late Pleistocene, by the later Late Pleistocene the region was dominated by tropical lowland evergreen rainforest, with a temporary return to drier conditions and more grassy vegetation during the Last Glacial Maximum (Louys and Roberts, 2020). Thus, the inhabitants of the regions around Trinil and Niah Cave during this period may have been engaged in broadly similar subsistence activities. A mobile hunting-gathering economy is consistent with the femoral morphology of Trinil 9.

The Deep Skull femur, very likely from a female, is much rounder (lower I_x/I_y) than Trinil 9. This is also consistent with differences in average femoral midshaft shape between males and females that are characteristic of *Homo* from the Middle Pleistocene through the early Holocene. Using the model in Figure 11, it might be suggested that such differences are a result of different body shapes, with the relatively broader hips of females creating relatively greater M-L bending of the femur and thus a decline in I_x/I_y (Ruff, 1995). However, the fact that very recent industrial populations, from any region, do not show sexual dimorphism in femoral midshaft shape (Ruff, 1987 and present study), yet still exhibit the same sexual dimorphism in pelvic morphology and body shape as earlier populations (Tague, 1989; Ruff, 1994; Kurki, 2011), argues for a different explanation. As shown previously (Ruff, 1987, 2019; Berner et al., 2018), among Holocene populations there is an association between degree of sexual dimorphism in femoral midshaft shape and sexual dimorphism in mobility. In hunting-gathering societies, males are generally more mobile than females; this difference (and differences in average femoral midshaft I_x/I_y) declines in agriculturalists, and is nonexistent in industrial societies, where mobility differences would be expected to be minimal. This pattern exists despite overall differences in body shape between populations. The present study confirms and extends this observation to additional regions and periods. The difference in femoral midshaft shape between Trinil 9 and the Deep Skull femur is thus consistent with that expected in an active foraging population with sexual division of labor. It is quite similar in this regard to the difference between the male and female specimens from Tam Hang, another Late Pleistocene inland site in Southeast Asia.

These findings also have implications for the sexing of other Late Pleistocene East Asian specimens. As noted earlier, the two Zhoukoudian Upper Cave femoral midshafts, UC 67 and 68, have very high I_x/I_y indices. Weidenreich (1941: Figure 45) identified both as male, without explanation. The present results support this attribution. Two of the three Maomaodong femora, GM7506 and GM7507, also have very A-P elongated midshafts, whereas the third Maomaodong femur, GM7508, is much rounder (see also Fig. 4), suggesting that the first two may be male and the third female. Estimated body masses of these specimens, and the two other Zhoukoudian Upper Cave specimens (UC 105 and 117), provide more mixed results. Weidenreich (1941: Figs. 40, 42) considered UC 105 to be male and UC 117 to be female, again without explanation. This would give body masses of 60.0, 67.5, and 69.0 kg for the three possible Upper Cave males, and 58.6 kg for the one possible female (SOM Table S2). The two possible Maomaodong males have estimated body masses of 59.8 and 63.6 kg, and the one possible female 59.8 kg, thus showing little overall variation as well as overlap between the sexes. Given normal overlap in both femoral midshaft cross-sectional shape and body size between males and females throughout the Pleistocene (Figs. 6 and 9), consideration of both types of characteristics may aid in the sexing of fragmentary specimens. More independently sexed specimens from this region and period would be helpful in further evaluating these observations.

The sample from Minatogawa, with relatively low values of femoral midshaft I_x/I_y and only slight sexual dimorphism in the index, despite deriving from a Late Pleistocene foraging population, would seem to be a partial exception to these general trends. However, as discussed in SOM S1, the specific environmental and subsistence characteristics of this sample, in particular a relatively insular culture and subsistence economy, may explain these findings.

Liang Bua 1 also has a relatively round femoral midshaft, as noted previously (Brown et al., 2004; Jungers et al., 2009b), although it is quite similar to that of the three Minatogawa females as well as one of the Tam Hang females. This could be a result of limited mobility, but it may also be affected by body shape. The estimated body mass of LB1, based on its femoral head breadth, is 31.4 kg [using its proximal tibial M-L breadth and the same reference sample (Ruff et al., 2018) yields a very similar estimate of 30.9 kg]. Combined with its estimated stature of 106 cm (Brown et al., 2004), this produces a BMI of 27.9 kg/m^2, which is much higher than that typical of modern tropical populations (Leonard and Katzmarzyk, 2010; also see above and SOM Table S5) and strongly implies a relatively wide body. Although the lack of a sacrum precludes direct assessment of total pelvic breadth, its large femoral bicondylar angle of 14° (Brown et al., 2004) also implies a relatively wide pelvis, which is consistent with its high BMI. This fits general patterns observed within modern populations, whereby within climatic zones variation in stature is much greater than variation in body breadth (Ruff, 1991, 1994). The relatively wide body of LB1 likely increased M-L bending loads on its femur (Ruff, 1995), which contributed to its low I_x/I_y value.

Some variation in relative body breadth between Southeast Asian and sub-Saharan African Late Pleistocene and early Holocene populations may also have contributed to observed differences in femoral diaphyseal shape. Pelves from Tam Hang and Minatogawa (Baba and Endo, 1982; Shackelford and Demeter, 2012) are wider than those from Late Stone Age South Africans (Stock, 2013), despite longer femoral lengths in the latter. Thus, a somewhat wider body relative to stature in some Late Pleistocene Southeast Asian populations may have contributed to generally lower sex-specific femoral midshaft I_x/I_y values compared to Late Stone Age South Africans (Fig. 7). The only moderately low BMI for Trinil 9 suggests that it, too, had a moderately narrow body. The fact that it still exhibits a relatively high femoral midshaft I_x/I_y value suggests a high level of mobility (Fig. 11).

A recent morphometric analysis of Pleistocene *Homo* femora concluded that "It is therefore unclear to what extent the distributions of diaphyseal shape among Middle and Late Pleistocene humans, as presented here, reflect the biomechanical effects of body proportions and activity levels versus population variation across the Old World during the Pleistocene" (Xing et al., 2021: 296). We would argue that all of these factors must be considered when interpreting variation in femoral cross-sectional diaphyseal shape, using the model in Figure 11. Variation due to population history is certainly a potential consideration, as illustrated by the possible differences in body form of some lower latitude populations from East Asia and sub-Saharan Africa discussed above. Cross-sectional shape of the femoral diaphysis is best understood as a product of the interaction between body shape, behavior (including sexual dimorphism in behavior), and in early *Homo*, hip biomechanics.

5. Conclusions

The Trinil 9 and 10 partial femora, dated to approximately 37–32 ka, add to our understanding of body size and behavior in the later Late Pleistocene of Southeast Asia. The overall morphology of the specimens indicates that they derive from anatomically modern *H. sapiens*. Cross-sectional diaphyseal shape of the better preserved Trinil 9 femur is consistent with that of an active mobile population. Based on systematic sexual dimorphism in shape throughout the Pleistocene, it was also most likely a male. Using a Pleistocene reference sample, its body mass can be estimated from its CA and estimated length as about 55 kg, and its stature as about 156 cm. In terms of both body size and behavior inferred from cross-sectional shape, it forms a male counterpart to the pene-contemporaneous Deep Skull femur from Niah Cave (estimated body mass 45 kg), which was most likely female. These imply the presence of relatively small-bodied, active hunting-gathering populations in the Sundaland region of Southeast Asia, together with possibly larger-bodied individuals or populations (e.g., the Wajak remains), during the later Late Pleistocene.

Data availability

All original and comparative Pleistocene hominin data used in the study are available in Table 6 and Supplementary Online Tables S2 and S3.

Declaration of competing interest

The authors declare that they have no competing interests.

Acknowledgments

Supported by the Treub Foundation; Stichting Nederlands Museum voor Paleoanthropologie en Praehistorie; Faculty of Archaeology, Leiden University; and the Dutch Research Council NWO (Grant number 016. Vidi.171.049 to J.C.J.). Collection of comparative data was supported by the National Science Foundation (grant numbers SBR-8919155, SBR-8919749, BSC-0642297). We are grateful to Frank Huffman for recognizing the importance of Trinil 9 and 10 and taking the initiative to study these bones, thereby laying the foundation for this work. We thank the following people for providing original data and/or cross-sectional images of Pleistocene and Holocene specimens: Peter Brown (Liang Bua), Isabel Crevecouer (Ishango), Tasuku Kimura (Jomon and modern Japanese), Laura Shackelford (Tam Hang, Cau Giat), Jay Stock (Late Stone Age South African, Andaman Islander), Chris Stojanowski and Paul Sereno (Gobero), Dan Temple (Jomon), and Song Xing (Zhoukoudian Upper Cave and Tianyuan). We thank Masaki Fujita, Laura Rodriguez, Karen Rosenberg, and Erik Trinkaus for clarifications regarding specimens and samples, and all of the many people who collaborated in collecting other comparative data, in particular Brigitte Holt, Markku Niskanen, Vladimir Sládek, and Margit Berner. We also thank the Indonesian Ministry of Research, Technology and Higher Education; Pusat Penelitian Arkeologi Nasional; and the staff of the Trinil Museum, notably Catur Hari Gumono and Agus Adi Widianto for pointing out the location of the Jacob excavations, and Natasja den Ouden for facilitating access to the Wajak remains.

Supplementary Online Material

Supplementary online material related to this article can be found at https://doi.org/10.1016/j.jhevol.2022.103252.

References

Akseer, N., Al-Gashm, S., Mehta, S., Mokdad, A., Bhutta, Z.A., 2017. Global and regional trends in the nutritional status of young people: A critical and neglected age group. Ann. N.Y. Acad. Sci. 1393, 3–20.

Baba, H., Endo, B., 1982. Postcranial skeleton of the Minatogawa man. In: Suzuki, H., Hanihara, T. (Eds.), The Minatogawa Man. The Upper Pleistocene Man from the Island of Okinawa. University of Tokyo, Tokyo, pp. 61–195.

Baba, H., Aziz, F., Watanabe, N., 1990. Morphology of the fossil hominid tibia from Sambungmacan, Java. Bull. Natn. Sci. Mus. Tokyo Ser. D 16, 9–18.

Bailey, K.V., 1962. Rural nutrition studies in Indonesia VI. Field studies of lactating women. Trop. Geogr. Med. 14, 11–19.

Barker, G., Barton, H., Bird, M., Daly, P., Datan, I., Dykes, A., Farr, L., Gilbertson, D., Harrisson, B., Hunt, C., Higham, T., Kealhofer, L., Krigbaum, J., Lewis, H., McLaren, S., Paz, V., Pike, A., Piper, P., Pyatt, B., Rabett, R., Reynolds, T., Rose, J., Rushworth, G., Stephens, M., Stringer, C., Thompson, J., Turney, C., 2007. The

'human revolution' in lowland tropical Southeast Asia: The antiquity and behavior of anatomically modern humans at Niah Cave (Sarawak, Borneo). J. Hum. Evol. 52, 243–261.
Berghuis, H., Veldkamp, A., Adhityatama, S., Hilgen, S.L., Sutisna, I., Barianto, D.H., Pop, E., Reimann, T., Yurnaldi, D., Ekowati, D.R., Vonhof, H.B., van Kolfschoten, T., Simanjuntak, T., Schoorl, J.M., Joordens, J.C.A., 2021. Hominin homelands of East Java: Revised stratigraphy and landscape reconstructions for Plio-Pleistocene Trinil. Quat. Sci. Rev. 260, 106912.
Bergmann, C., 1847. Uber die verhaltniesse der warmeokonomie der thiere zu ihrer grosse. Gottingen Stud. 1, 595–708.
Berner, M., Sládek, V., Holt, B., Niskanen, M., Ruff, C.B., 2018. Sexual dimorphism. In: Ruff, C.B. (Ed.), Skeletal Variation and Adaptation in Europeans: Upper Paleolithic to the Twentieth Century. Wiley-Blackwell, Hoboken, pp. 133–161.
Black, R.E., Victora, C.G., Walker, S.P., Bhutta, Z.A., Christian, P., de Onis, M., Ezzati, M., Grantham-McGregor, S., Katz, J., Martorell, R., Uauy, R., Maternal, Child Nutrition Study, G., 2013. Maternal and child undernutrition and overweight in low-income and middle-income countries. Lancet 382, 427–451.
Brown, J.H., West, G.B., 2000. Scaling in Biology. Oxford University Press, Oxford.
Brown, P., Sutikna, T., Morwood, M.J., Soejono, R.P., Jatmiko, Saptomo, E.W., Due, R.A., 2004. A new small-bodied hominin from the Late Pleistocene of Flores, Indonesia. Nature 431, 1055–1061.
Brumm, A., Jensen, G.M., van den Bergh, G.D., Morwood, M.J., Kurniawan, I., Aziz, F., Storey, M., 2010. Hominins on Flores, Indonesia, by one million years ago. Nature 464, 748–752.
Calder III, W.A., 1984. Size, Function, and Life History. Cambridge University Press, Cambridge.
Campbell, M.C., Tishkoff, S.A., 2008. African genetic diversity: Implications for human demographic history, modern human origins, and complex disease mapping. Annu. Rev. Genomics Hum. Genet. 9, 403–433.
Carretero, J.M., Rodríguez, L., Garcia-González, R., Arsuaga, J.L., Gómez-Olivencia, A., Lorenzo, C., Bonmatí, A., Gracia, A., Martínez, I., Quam, R., 2012. Stature estimation from complete long bones in the Middle Pleistocene humans from the Sima de los Huesos, Sierra de Atapuerca (Spain). J. Hum. Evol. 62, 242–255.
Chuan, T.K., Hartono, M., Kumar, N., 2010. Anthropometry of the Singaporean and Indonesian populations. Int. J. Ind. Ergon. 40, 757–766.
Churchill, S.E., Holliday, T.W., Carlson, K.J., Jashashvili, T., Macias, M.E., Mathews, S., Sparling, T.L., Schmid, P., de Ruiter, D.J., Berger, L.R., 2013. The upper limb of *Australopithecus sediba*. Science 340, 1233477.
Cleveland, W.S., 1979. Robust locally weighted regression and smoothing scatterplots. J. Am. Stat. Assoc. 74, 829–836.
Coban, S.B., Lucka, F., Palenstijn, W.J., Van Loo, D., Batenburg, K.J., 2020. Explorative imaging and its implementation at the FleX-ray laboratory. J. Imaging 6, 18.
Corny, J., Garong, A.M., Sémah, F., Dizon, E.Z., Bolunia, M.J.L.A., Bautista, R., Détroit, F., 2016. Paleoanthropological significance and morphological variability of the human bones and teeth from Tabon Cave. Quat. Int. 416, 210–218.
Curnoe, D., Ji, X., Liu, W., Bao, Z., Tacon, P.S., Ren, L., 2015. A hominin femur with archaic affinities from the Late Pleistocene of Southwest China. PLoS One 10, e0143332.
Curnoe, D., Datan, I., Tacon, P.S.C., Ung, C.L.M., Sauffi, M.S., 2016. Deep Skull from Niah Cave and the Pleistocene peopling of Southeast Asia. Front. Ecol. Evol. 4, 75.
Curnoe, D., Datan, I., Goh, H.M., Sauffi, M.S., 2019. Femur associated with the Deep Skull from the west mouth of the Niah Caves (Sarawak, Malaysia). J. Hum. Evol. 127, 133–148.
Curnoe, D., Datan, I., Goh, H.M., Bin Sauffi, M.S., Ruff, C.B., 2021. Further analyses of the Deep Skull femur from Niah Caves, Malaysia. J. Hum. Evol. 161, 103089.
Davies, T.G., Stock, J.T., 2014a. Human variation in the perioteal geometry of the lower limb: Signatures of behaviour among human Holocene populations. In: Carlson, K., Marchi, D. (Eds.), Reconstructing Mobility: Interpreting Behavior from Skeletal Adaptations and Environmental Interactions. Springer, New York, pp. 67–90.
Davies, T.G., Stock, J.T., 2014b. The influence of relative body breadth on the diaphyseal morphology of the human lower limb. Am. J. Hum. Biol. 26, 822–835.
Day, M.H., 1984. The postcranial remains of *Homo erectus* from Africa, Asia, and possibly Europe. Cour. Forsch. Inst. Senckenberg 69, 113–121.
Day, M.H., 1986. Bipedalism: Pressures, origins and modes. In: Wood, B., Martin, L., Andrews, P. (Eds.), Major Topics in Primate and Human Evolution. Cambridge University Press, Cambridge, pp. 188–202.
Day, M.H., Molleson, T.I., 1973. The Trinil femora. In: Day, M. (Ed.), Human Evolution. Society for the Study of Human Biology Symposium Series, vol. 11. Taylor & Francis, London, pp. 127–154.
de Lumley, M.-A., 1993. Le Pithecanthrope de Java: Connus and inconnus. Les Dossiers d'Archéologie 184, 26–29.
Dennell, R., Martinón-Torres, M., Bermúdez de Castro, J.-M., Xing, G., 2020. A demographic history of Late Pleistocene China. Quat. Int. 559, 4–13.
Détroit, F., Dizon, E., Falguères, C., Hameau, S., Ronquillo, W., Sémah, F., 2004. Upper Pleistocene *Homo sapiens* from the Tabon cave (Palawan, The Philppines): Description and dating of new discoveries. C.R. Palevol 3, 705–712.
Détroit, F., Corny, J., Dizon, E.Z., Mijares, A.S., 2013. "Small size" in the Philippine human fossil record: Is it meaningful for a better understanding of the evolutionary history of the negritos? Hum. Biol. 85, 45–65.
Détroit, F., Mijares, A.S., Corny, J., Daver, G., Zanolli, C., Dizon, E., Robles, E., Grun, R., Piper, P.J., 2019. A new species of *Homo* from the Late Pleistocene of the Philippines. Nature 568, 181–186.
Dubois, E., 1893. Palaeontologische onderzoekingen op Java. Verslag van het Mijnwezen Batavia 3 (1892), 10–14. (Translated by W.E. Meikle and S.T. Parker, 1994. Naming our Ancestors. An Anthology of Hominid Taxonomy. Waveland Press, Prospect Heights, pp. 1936–1930).
Dubois, E., 1894. *Pithecanthropus erectus*, eine menschednahnliche Uebergangsform aus Java. National Press, Batavia.
Dubois, E., 1932. The distinct organization of *Pithecanthropus* of which the femur bears evidence, now confirmed from other individuals of the described species. Proc. K. Ned. Akad. Wet. 35, 716–722.
Dubois, E., 1934. New evidence of the distinct organization of *Pithecanthropus*. Proc. K. Ned. Akad. Wet. 37, 139–145.
Eveleth, P.B., Tanner, J.M., 1976. Worldwide Variation in Human Growth. Cambridge University Press, Cambridge.
FEI Visualization Sciences Group, 2015. Avizo Lite 9.0.1. FEI Company, Hillsboro, Oregon.
Feldesman, M.R., Lundy, J.K., 1988. Stature estimates for some African Plio-Pleistocene fossil hominids. J. Hum. Evol. 17, 583–596.
Fellmann, C.D., 2004. Estimation of femoral length and stature in fossil and modern hominins: A test of methods. Master's Thesis, Rutgers University.
Feuerriegel, E.M., Green, D.J., Walker, C.S., Schmid, P., Hawks, J., Berger, L.R., Churchill, S.E., 2017. The upper limb of *Homo naledi*. J. Hum. Evol. 104, 155–173.
Foster, F., Collard, M., 2013. A reassessment of Bergmann's rule in modern humans. PLoS One 8, e72269.
Friedl, L., Eisova, S., Holliday, T.W., 2016. Re-evaluation of Pleistocene and Holocene long bone robusticity trends with regards to age-at-death estimates and size standardization procedures. J. Hum. Evol. 97, 109–122.
Gardezi, T., da Silva, J., 1999. Diversity in relation to body size in mammals: A comparative study. Am. Nat. 153, 110–123.
Garvin, H.M., Elliott, M.C., Delezene, L.K., Hawks, J., Churchill, S.E., Berger, L.R., Holliday, T.W., 2017. Body size, brain size, and sexual dimorphism in *Homo naledi* from the Dinaledi Chamber. J. Hum. Evol. 111, 119–138.
Gocha, T.P., Vercellotti, G., McCormick, L.E., Van Deest, T.L., 2013. Formulae for estimating skeletal height in modern South-East Asians. J. Forensic Sci. 58, 1279–1283.
Grabowski, M., Hatala, K.G., Jungers, W.L., Richmond, B.G., 2015. Body mass estimates of hominin fossils and the evolution of human body size. J. Hum. Evol. 85, 75–93.
Grimaud-Hervé, D., Valentin, F., Sémah, F., Sémah, A.M., Djubiantono, T., Widianto, H., 1994. Le fémur humain Kresna 11 comparé à ceux de Trinil. C.R. Acad. Sci. Ser. II 318, 1139–1144.
Grün, R., Aubert, M., Joannes-Boyau, R., Moncel, M.-H., 2008. High resolution analysis of uranium and thorium concentration as well as U-series isotope distributions in a Neanderthal tooth from Payre (Ardèche, France) using laser ablation ICP-MS. Geochim. Cosmochim. Acta 72, 5278–5290.
Harcourt-Smith, W.E., Throckmorton, Z., Congdon, K.A., Zipfel, B., Deane, A.S., Drapeau, M.S., Churchill, S.E., Berger, L.R., DeSilva, J.M., 2015. The foot of *Homo naledi*. Nat. Commun. 6, 8432.
Hens, S.M., Konigsberg, L.W., Jungers, W.L., 2000. Estimating stature in fossil hominids: Which regression model and reference sample to use? J. Hum. Evol. 38, 767–784.
Herries, A., Murszewski, A., Pickering, R., Mallett, T., Joannes-Boyau, R., Armstrong, B., Adams, J., Baker, S., Blackwood, A., Penzokajewski, P., Kappen, P., Leece, A.B., Martin, J., Rovinsky, D., Boschian, G., 2018. Geoarchaeological and 3D visualisation approaches for contextualising in-situ fossil bearing palaeokarst in South Africa: A case study from the ~2.61 Ma Drimolen Makondo. Quat. Int. 483, 90–110.
Holliday, T.W., Ruff, C.B., 1997. Ecogeographic patterning and stature prediction in fossil hominids: Comment on Feldesman and Fountain. Am. J. Phys. Anthropol. 103, 137–140.
Holt, B., Whittey, E., 2019. The impact of terrain on lower limb bone structure. Am. J. Phys. Anthropol. 168, 729–743.
Holt, B., Whittey, E., Niskanen, M., Sládek, V., Berner, M., Ruff, C.B., 2018. Temporal and geographic variation in robusticity. In: Ruff, C.B. (Ed.), Skeletal Variation and Adaptation in Europeans: Upper Paleolithic to the Twentieth Century. Wiley-Blackwell, New York, pp. 91–132.
Indriati, E., 2004. Indonesian fossil hominid discoveries from 1889 to 2003: Catalogue and problems. In: Akiyama, S., Hakubutsukan, K.K. (Eds.), Proceedings of the 5th and 6th Symposia on Collection Building and Natural History Studies in Asia and the Pacific Rim, Natl. Sci. Mus. Monogr. Tokyo, pp. 163–177.
Ingicco, T., van den Bergh, G.D., Jago-On, C., Bahain, J.J., Chacón, M.G., Amano, N., Forestier, H., King, C., Manalo, K., Nomade, S., Pereira, A., Reyes, M.C., Sémah, A.M., Shao, Q., Voinchet, P., Falguères, C., Albers, P.C.H., Lising, M., Lyras, G., Yurnaldi, D., Rochette, P., Bautista, A., de Vos, J., 2018. Earliest known hominin activity in the Philippines by 709 thousand years ago. Nature 557, 233–237.
Jacob, T., 1973. Palaeoanthropological discoveries in Indonesia with special reference to the finds of the last two decades. J. Hum. Evol. 2, 473–485.
Jacob, T., 1975. Indonesia. In: Oakley, K.P., Campbell, B.G., Molleson, T.I. (Eds.), Catalogue of Fossil Hominids, Part III: Americas, Asia, Australasia. British Museum of Natural History, London, pp. 103–124.
Jacob, T., 1978. New finds of Lower and Middle Pleistocene hominines from Indonesia and an examination of their antiquity. In: Fumiko, I.-S. (Ed.), Early Paleolithic in South and East Asia. De Gruyter Mouton, New York, pp. 13–22.

Jacobs, K., 1992. Estimating femur and tibia length from fragmentary bones: An evaluation of Steele's (1970) method using a prehistoric European sample. Am. J. Phys. Anthropol. 89, 333–345.
Jungers, W.L., Grabowski, M., Hatala, K.G., Richmond, B.G., 2016. The evolution of body size and shape in the human career. Philos. Trans. R. Soc. Lond. B Biol. Sci. 371.
Jungers, W.L., Harcourt-Smith, W.E.H., Wunderlich, R.E., Tocheri, M.W., Larson, S.G., Sutikna, T., Due, R.A., Morwood, M.J., 2009a. The foot of *Homo floresiensis*. Nature 459, 81–84.
Jungers, W.L., Larson, S.G., Harcourt-Smith, W., Morwood, M.J., Sutikna, T., Awe, R.D., Djubiantono, T., 2009b. Descriptions of the lower limb skeleton of *Homo floresiensis*. J. Hum. Evol. 57, 538–554.
Katzmarzyk, P.T., Leonard, W.R., 1998. Climatic influences on human body size and proportions: Ecological adaptations and secular trends. Am. J. Phys. Anthropol. 106, 483–503.
Kennedy, G.E., 1983. Some aspects of femoral morphology in *Homo erectus*. J. Hum. Evol. 12, 587–616.
Kimura, T., Takahashi, H., 1992. Cross-sectional geometry of the Minatogawa limb bones. In: Akazawa, T., Aoki, K., Kimura, T. (Eds.), The Evolution and Dispersal of Modern Humans in Asia. Hokusen-Sha, Tokyo, pp. 305–320.
Kivell, T.L., Deane, A.S., Tocheri, M.W., Orr, C.M., Schmid, P., Hawks, J., Berger, L.R., Churchill, S.E., 2015. The hand of *Homo naledi*. Nat. Commun. 6, 8431.
Kurki, H.K., 2011. Pelvic dimorphism in relation to body size and body size dimorphism in humans. J. Hum. Evol. 61, 631–643.
Leonard, W.R., Katzmarzyk, P.T., 2010. Body size and shape: Climatic and nutritional influences on human body morphology. In: Meuehlenbein, M.P. (Ed.), Human Evolutionary Biology. Cambridge University Press, Cambridge, pp. 157–169.
Louys, J., Roberts, P., 2020. Environmental drivers of megafauna and hominin extinction in Southeast Asia. Nature 586, 402–406.
Lovejoy, C.O., Latimer, B., Suwa, G., Asfaw, B., White, T.D., 2009. Combining prehension and propulsion: The foot of *Ardipithecus ramidus*. Science 326, 72e71-78.
Mahakkanukrauh, P., Khanpetch, P., Prasitwattanseree, S., Vichairat, K., Troy Case, D., 2011. Stature estimation from long bone lengths in a Thai population. Forensic Sci. Int. 210, 279 e271–277.
Marchi, D., Walker, C.S., Wei, P., Holliday, T.W., Churchill, S.E., Berger, L.R., DeSilva, J.M., 2017. The thigh and leg of *Homo naledi*. J. Hum. Evol. 104, 174–204.
McHenry, H.M., 1992. Body size and proportions in early hominids. Am. J. Phys. Anthropol. 87, 407–431.
Mijares, A.S., Detroit, F., Piper, P., Grun, R., Bellwood, P., Aubert, M., Champion, G., Cuevas, N., De Leon, A., Dizon, E., 2010. New evidence for a 67,000-year-old human presence at Callao Cave, Luzon, Philippines. J. Hum. Evol. 59, 123–132.
Morwood, M.J., Brown, P., Jatmiko, Sutikna, T., Saptomo, E.W., Westaway, K.E., Due, R.A., Roberts, R.G., Maeda, T., Wasisto, S., Djubiantono, T., 2005. Further evidence for small-bodied hominins from the Late Pleistocene of Flores, Indonesia. Nature 437, 1012–1017.
Niskanen, M., Junno, J.A., Maijanen, H., Holt, B., Sládek, V., Berner, M., 2018. Can we refine body mass estimations based on femoral head breadth? J. Hum. Evol. 115, 112–121.
O'Connell, J.F., Allen, J., Williams, M.A.J., Williams, A.N., Turney, C.S.M., Spooner, N.A., Kamminga, J., Brown, G., Cooper, A., 2018. When did *Homo sapiens* first reach Southeast Asia and Sahul? Proc. Natl. Acad. Sci. USA 115, 8482–8490.
Pearson, O.M., Peterson, T.R., Sparacello, V., Daneshvari, S.R., Grine, F.E., 2014. Activity, "body shape," and cross-sectional geometry of the femur and tibia. In: Carlson, K., Marchi, D. (Eds.), Reconstructing Mobility: Interpreting Behavior from Skeletal Adaptations and Environmental Interactions. Springer, New York, pp. 133–151.
Puymerail, L., Ruff, C.B., Bondioli, L., Widianto, H., Trinkaus, E., Macchiarelli, R., 2012. Structural analysis of the Kresna 11 *Homo erectus* femoral shaft (Sangiran, Java). J. Hum. Evol. 63, 741–749.
Raxter, M.H., Auerbach, B.M., Ruff, C.B., 2006. A revision of the Fully technique for estimating statures. Am. J. Phys. Anthropol. 130, 374–384.
Rightmire, G.P., 1986. Body size and encephalization in *Homo erectus*. Anthropos (Brno). 23, 139–149.
Rizal, Y., Westaway, K.E., Zaim, Y., van den Bergh, G.D., Bettis, E.A., Morwood, M.J., Huffman, O.F., Grun, R., Joannes-Boyau, R., Bailey, R.M., Sidarto, Westaway, M.C., Kurniawan, I., Moore, M.W., Storey, M., Aziz, F., Suminto, Zhao, J.X., Aswan, Sipola, M.E., Larick, R., Zonneveld, J.P., Scott, R., Putt, S., Ciochon, R.L., 2020. Last appearance of *Homo erectus* at Ngandong, Java, 117,000-108,000 years ago. Nature 577, 381–385.
Roberts, D.F., 1953. Body weight, race and climate. Am. J. Phys. Anthropol. 11, 533–558.
Roberts, D.F., 1978. Climate and Human Variability, 2nd ed. Cummings, Menlo Park.
Rosenberg, K.R., Lu, Z., Ruff, C.B., 1999. Body size, body proportions and encephalization in the Jinniushan specimen. Am. J. Phys. Anthropol. Suppl. 28, 235.
Ruff, C.B., 1987. Sexual dimorphism in human lower limb bone structure: Relationship to subsistence strategy and sexual division of labor. J. Hum. Evol. 16, 391–416.
Ruff, C.B., 1991. Climate, body size and body shape in hominid evolution. J. Hum. Evol. 21, 81–105.
Ruff, C.B., 1994. Morphological adaptation to climate in modern and fossil hominids. Yearb. Phys. Anthropol. 37, 65–107.
Ruff, C.B., 1995. Biomechanics of the hip and birth in early *Homo*. Am. J. Phys. Anthropol. 98, 527–574.
Ruff, C.B., 2002. Long bone articular and diaphyseal structure in Old World monkeys and apes, I: Locomotor effects. Am. J. Phys. Anthropol. 119, 305–342.
Ruff, C.B., 2005. Mechanical determinants of bone form: Insights from skeletal remains. J. Musculoskelet. Neuronal Interact. 5, 202–212.
Ruff, C.B., 2009. Relative limb strength and locomotion in Homo habilis. Am. J. Phys. Anthropol. 138, 90–100.
Ruff, C.B., 2018. Skeletal Variation and Adaptation in Europeans: Upper Paleolithic to the Twentieth Century. Wiley-Blackwell, Hoboken.
Ruff, C.B., 2019. Biomechanical analyses of archaeological human skeletal samples. In: Katzenburg, M.A., Grauer, A.L. (Eds.), Biological Anthropology of the Human Skeleton, 3rd ed. John Wiley & Sons, New York, pp. 189–224.
Ruff, C.B., n.d. MomentMacro: https://fae.johnshopkins.edu/chris-ruff/.
Ruff, C.B., Hayes, W.C., 1983. Cross-sectional geometry of Pecos Pueblo femora and tibiae - a biomechanical investigation. I. Method and general patterns of variation. Am. J. Phys. Anthropol. 60, 359–381.
Ruff, C.B., Larsen, C.S., 2014. Long bone structural analyses and reconstruction of past mobility: A historical review. In: Carlson, K., Marchi, D. (Eds.), Reconstructing Mobility: Interpreting Behavior from Skeletal Adaptations and Environmental Interactions. Springer, New York, pp. 13–29.
Ruff, C.B., Trinkaus, E., Walker, A., Larsen, C.S., 1993. Postcranial robusticity in *Homo*, I: Temporal trends and mechanical interpretation. Am. J. Phys. Anthropol. 91, 21–53.
Ruff, C.B., Holt, B.M., Niskanen, M., Sládek, V., Berner, M., Garofalo, E., Garvin, H.M., Hora, M., Maijanen, H., Niinimaki, S., Salo, K., Schuplerova, E., Tompkins, D., 2012. Stature and body mass estimation from skeletal remains in the European Holocene. Am. J. Phys. Anthropol. 148, 601–617.
Ruff, C.B., Holt, B.M., Niskanen, M., Sládek, V., Berner, M., Garofalo, E., Garvin, H.M., Hora, M., Junno, J.-A., Schuplerova, E., Vilkama, R., Whittey, E., 2015a. Gradual decline in mobility with the adoption of food production in Europe. Proc. Natl. Acad. Sci. USA 112, 7147–7152.
Ruff, C.B., Puymerail, L., Macchiarelli, R., Sipla, J., Ciochon, R.L., 2015b. Structure and composition of the Trinil femora: Functional and taxonomic implications. J. Hum. Evol. 80, 147–158.
Ruff, C.B., Burgess, M.L., Ketcham, R.A., Kappelman, J., 2016. Limb bone structural proportions and locomotor behavior in A.L. 288-1 ("Lucy"). PLoS One 11, e0166095.
Ruff, C.B., Burgess, M.L., Squyres, N., Junno, J.-A., Trinkaus, E., 2018. Lower limb articular scaling and body mass estimation in Pliocene and Pleistocene hominins. J. Hum. Evol. 115, 85–111.
Ruff, C.B., Niskanen, M., Maijanen, H., Mays, S., 2019. Effects of age and body proportions on stature estimation. Am. J. Phys. Anthropol. 168, 370–377.
Santa Luca, A.P., 1980. The Ngandong fossil hominids: A comparative study of a Far Eastern *Homo erectus* group. Yale University Press, New Haven.
Scerri, E.M.L., Thomas, M.G., Manica, A., Gunz, P., Stock, J.T., Stringer, C.B., Grove, M., Groucutt, H.S., Timmermann, A., Rightmire, G.P., d'Errico, F., Tryon, C.A., Drake, N., Brooks, A.S., Dennell, R., Durbin, R., Henn, B.M., Lee-Thorp, J.A., deMenocal, P.B., Petraglia, M.D., Thompson, J.C., Scally, A., Chikhi, L., 2018. Did our species evolve in subdivided populations across Africa, and why does it matter? Trends Ecol. Evol. 33, 582–594.
Schmidt-Nielson, K., 1984. Scaling: Why is Animal Size So Important? Cambridge University Press, Cambridge.
Shackelford, L.L., 2007. Regional variation in the postcranial robusticity of Late Upper Paleolithic humans. Am. J. Phys. Anthropol. 133, 655–668.
Shackelford, L., Demeter, F., 2012. The place of Tam Hang in Southeast Asian human evolution. C. R. Palevol 11, 97–115.
Shang, H., Trinkaus, E., 2010. The Early Modern Human from Tianyuan Cave, China. Texas A&M University Press, College Station, TX.
Shaw, C.N., Stock, J.T., 2011. The influence of body proportions on femoral and tibial midshaft shape in hunter-gatherers. Am. J. Phys. Anthropol. 144, 22–29.
Steele, D.G., 1970. Estimation of stature from fragments of long limb bones. In: Stewart, T.D. (Ed.), Personal Identification in Mass Disasters. National Museum of Natural History, Smithsonian Institution, Washington, DC, pp. 85–97.
Steele, D.G., McKern, T.W., 1969. A method for assessment of maximum long bone length and living stature from fragmentary long bones. Am. J. Phys. Anthropol. 31, 215–227.
Stock, J.T., 2006. Hunter-gatherer postcranial robusticity relative to patterns of mobility, climatic adaptation, and selection for tissue economy. Am. J. Phys. Anthropol. 131, 194–204.
Stock, J.T., 2013. The skeletal phenotype of "negritos" from the Andaman Islands and Philippines relative to global variation among hunter-gatherers. Hum. Biol. 85, 67–94.
Stock, J., Pfeiffer, S., 2001. Linking structural variability in long bone diaphyses to habitual behaviors: Foragers from the southern African Later Stone Age and the Andaman Islands. Am. J. Phys. Anthropol. 115, 337–348.
Storm, P., 1995. The evolutionary significance of the Wajak skulls. Scripta Geol. 110, 1–247.
Storm, P., Wood, R., Stringer, C., Bartsiokas, A., de Vos, J., Aubert, M., Kinsley, L., Grun, R., 2013. U-series and radiocarbon analyses of human and faunal remains from Wajak, Indonesia. J. Hum. Evol. 64, 356–365.
SYSTAT13, 2009. SYSTAT Software, Inc., Chicago.
Tague, R.G., 1989. Variation in pelvic size between males and females. Am. J. Phys. Anthropol. 80, 59–71.
Temple, D.H., 2008. What can variation in stature reveal about environmental differences between prehistoric Jomon foragers? Understanding the impact of systemic stress on developmental stability. Am. J. Hum. Biol. 20, 431–439.

Theunissen, B., 1989. Eugene Dubois and the Ape-Man from Java. Kluwer, Dordrecht.
Tocheri, M.W., Orr, C.M., Larson, S.G., Sutikna, T., Jatmiko, Saptomo, E.W., Due, R.A., Djubiantono, T., Morwood, M.J., Jungers, W.L., 2007. The primitive wrist of *Homo floresiensis* and its implications for hominin evolution. Science 317, 1743–1745.
Trinkaus, E., Ruff, C.B., 2012. Femoral and tibial diaphyseal cross-sectional geometry in Pleistocene *Homo*. PaleoAnthropology 2012, 13–62.
Trotter, M., Gleser, G.C., 1952. Estimation of stature from long bones of American whites and Negroes. Am. J. Phys. Anthropol. 10, 463–514.
van den Bergh, G.D., Kaifu, Y., Kurniawan, I., Kono, R.T., Brumm, A., Setiyabudi, E., Aziz, F., Morwood, M.J., 2016a. *Homo floresiensis*-like fossils from the early Middle Pleistocene of Flores. Nature 534, 245–248.
van den Bergh, G.D., Li, B., Brumm, A., Grun, R., Yurnaldi, D., Moore, M.W., Kurniawan, I., Setiawan, R., Aziz, F., Roberts, R.G., Suyono, Storey, M., Setiabudi, E., Morwood, M.J., 2016b. Earliest hominin occupation of Sulawesi, Indonesia. Nature 529, 208–211.
Voris, H.K., 2000. Maps of Pleistocene sea levels in Southeast Asia: Shorelines, river systems, and time durations. J. Biogeogr. 27, 1153–1167.
Ward, C.V., Feibel, C.S., Hammond, A.S., Leakey, L.N., Moffett, E.A., Plavcan, J.M., Skinner, M.M., Spoor, F., Leakey, M.G., 2015. Associated ilium and femur from Koobi Fora, Kenya, and postcranial diversity in early *Homo*. J. Hum. Evol. 81, 48–67.
Warden, S.J., Mantila Roosa, S.M., Kersh, M.E., Hurd, A.L., Fleisig, G.S., Pandy, M.G., Fuchs, R.K., 2014. Physical activity when young provides lifelong benefits to cortical bone size and strength in men. Proc. Natl. Acad. Sci. USA 111, 5337–5342.
Weaver, T.D., 2003. The shape of the Neandertal femur is primarily the consequence of a hyperpolar body form. Proc. Natl. Acad. Sci. USA 100, 6926–6929.
Wei, P., Lu, H., Carlson, K.J., Zhang, H., Hui, J., Zhu, M., He, K., Jashashvili, T., Zhang, X., Yuan, H., Xing, S., 2020. The upper limb skeleton and behavioral lateralization of modern humans from Zhaoguo Cave, southwestern China. Am. J. Phys. Anthropol. 173, 671–696.
Wei, P., Weng, Z., Carlson, K.J., Cao, B., Jin, L., Liu, W., 2021. Late Pleistocene partial femora from Maomaodong, southwestern China. J. Hum. Evol. 155, 102977.
Weidenreich, F., 1941. The extremity bones of *Sinanthropus pekinensis*. Paleontol. Sin. Ser. D 5, 1–150.
Wescott, D.J., 2014. The relationship between femur shape and terrestrial mobility patterns. In: Carlson, K., Marchi, D. (Eds.), Reconstructing Mobility: Interpreting Behavior from Skeletal Adaptations and Environmental Interactions. Springer, New York, pp. 111–132.
Widiasmoro, A.S., 1991. Excursion Guide Trinil, Perning. International Trinil Centennial Colloquium, Surabaya.
Will, M., Stock, J.T., 2015. Spatial and temporal variation of body size among early *Homo*. J. Hum. Evol. 82, 15–33.
Will, M., Pablos, A., Stock, J.T., 2017. Long-term patterns of body mass and stature evolution within the hominin lineage. R. Soc. Open Sci. 4, 171339.
Will, M., Krapp, M., Stock, J.T., Manica, A., 2021. Different environmental variables predict body and brain size evolution in *Homo*. Nat. Commun. 12, 4116.
Woodroffe, C.D., Short, S.A., Stoddart, D.R., Spencer, T., Harmon, R.S., 1991. Stratigraphy and chronology of Late Pleistocene reefs in the Southern Cook Islands, South Pacific. Quat. Res. 35, 246–263.
Xing, S., Carlson, K.J., Wei, P., He, J., Liu, W., 2018. Morphology and structure of *Homo erectus* humeri from Zhoukoudian, Locality 1. PeerJ 6, e4279.
Xing, S., Wu, X.J., Liu, W., Pei, S.W., Cai, Y.J., Tong, H.W., Trinkaus, E., 2021. Middle Pleistocene human femoral diaphyses from Hualongdong, Anhui Province, China. Am. J. Phys. Anthropol. 174, 285–298.
Zipfel, B., DeSilva, J.M., Kidd, R.S., Carlson, K.J., Churchill, S.E., Berger, L.R., 2011. The foot and ankle of *Australopithecus sediba*. Science 333, 1417–1420.